Rearrangements of 2-Nitrobenzyl Compounds. 1. Potential Energy Surface of 2-Nitrotoluene and Its Isomers Explored with ab Initio and Density Functional Theory Methods

Yuri V. Il'ichev*,† and Jakob Wirz

Contribution from Institut für Physikalische Chemie der Universität Basel, Klingelbergstrasse 80, CH-4056 Basel, Switzerland

Received: January 20, 2000; In Final Form: April 26, 2000

Reaction paths leading from 2-nitrotoluene (**1**) to 2-nitrosobenzyl alcohol (**4**) were investigated by using ab initio and density functional theory. Overall, 25 minima and 12 transition states were located for molecules of composition $C_7H_7NO_2$. Nine conformational minima were found for **4**, all being slightly lower in energy than **1**. The lowest-energy path from **1** to **4** was predicted to have an overall activation energy of 51.7 kcal mol^{-1} at the B3LYP/6-311+G(2d,p)//B3LYP/6-31G(d,p) level of theory. The rate-determining step is a 1,3-hydrogen shift between two oxygen atoms in the *aci*-form **2**. The activation barrier of 20.3 kcal mol^{-1} predicted for this shift is substantially higher than that of 9.7 kcal mol^{-1} for the retautomerization **2** → **1**. To account for reaction paths involving ionization of the moderately strong acid **2** in aqueous solution, anions obtained by deprotonation of **1**−**4** were studied. A common anion **2**$^-$ was found by CH-deprotonation of **1** and by OH-deprotonation of two *aci*-isomers **2**. An anion **3**$^-$ was obtained by deprotonation of benzisoxazoline **3** and nitrone **6**. A single conformer **4**$^-$ was located by deprotonation of **4**. At the B3LYP/6-311+G(2d,p) level the activation barrier of 39.2 kcal mol^{-1} for the reaction **2**$^-$ → **3**$^-$ is much higher than that of 18.4 kcal mol^{-1} for the cyclization of the neutral *aci*-form, *trans*-**2** → **3a**. The barrier height for the latter reaction was reproduced within 1.0 kcal mol^{-1} by calculating QCISD(T)/6-31G(d,p) energies at the B3LYP and MP2/6-31G(d) geometries. On the other hand, the reaction **3**$^-$ → **4**$^-$ is expected to be very facile in contrast to ring opening in the neutral species, **3** → **4**. These results indicate that the cyclization **2** → **3** is acid-catalyzed around neutral pH and that the subsequent ring opening **3** → **4** is base-catalyzed.

Introduction

The 2-nitrobenzyl group is widely used as a photosensitive protector in organic synthesis,[1] polymer chemistry,[2] microelectronics,[3] and biochemistry.[4−7] 2-Nitrobenzyl compounds are currently major photolabile precursors used to obtain temporal and spatial control over the release of biologically active compounds.[8] Nevertheless, the mechanism of the photoinduced reaction and the ensuing substituent and environmental effects are poorly understood (see Discussion). In this work, density functional theory (DFT) was applied to explore the potential energy surface connecting 2-nitrotoluene (**1**) to the *aci*-form **2**, benzisoxazoline (**3**), and 2-nitrosobenzyl alcohol (**4**), Scheme 1. The parent compound **1** was selected as a tractable model for nitrobenzyl derivatives of practical importance, although its *aci*-form **2**, also referred to as a quinonoid intermediate, predominantly retautomerizes to **1** when generated by photolysis of **1** in aqueous solution.[9] Computational results for substituent effects on the cyclization of the *aci*-form **2** → **3** will be reported in a forthcoming paper. To account for acid dissociation in aqueous solution, reactions of the deprotonated species were also considered. Essential conclusions regarding the thermal and photoinduced reactions of nitrobenzyl compounds may be drawn from the results presented.

SCHEME 1: Photoinduced Reaction of 2-Nitrotoluene

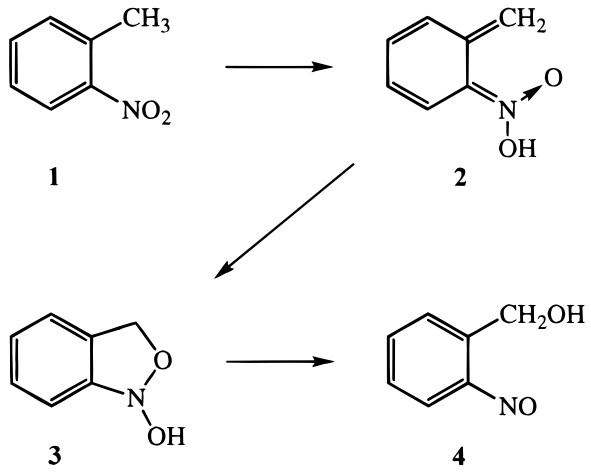

Methods of Calculation

All calculations were performed with the GAUSSIAN 94[10] and 98[11] packages of programs. Geometries were initially optimized at the SCF level of theory with the standard 6-31G(d) basis set. To include electron correlation, more sophisticated ab initio methods and techniques based on DFT were employed. Geometry optimization for all stationary points was done at the B3LYP level of theory. To test the performance of different exchange-correlation functionals, the geometry of **1** was also fully optimized with two other methods (BHLYP and B3PW91). B3LYP and B3PW91 are combinations of Becke's three-parameter exchange functional[12] with the slightly modified Lee−Yang−Parr[13] (LYP) and Perdew−Wang[14] (PW91) correlation functional, respectively. BHLYP denotes Becke's hybrid half-and-half method[15] combined with the LYP correlation functional

† Present address: P. M. Gross Chemical Laboratory, Department of Chemistry, Duke University, Box 90349, Durham, NC 27708-0348; e-mail, ilitchev@chem.duke.edu.

10.1021/jp000261v CCC: $19.00
Published on Web 07/27/2000

SCHEME 2: Atom Numbering Scheme for 2-Nitrotoluene (1), the *aci*-Forms (2), the Bicyclic Intermediate (3), and the Most Stable Conformer of 2-Nitrosobenzyl Alcohol (4a)

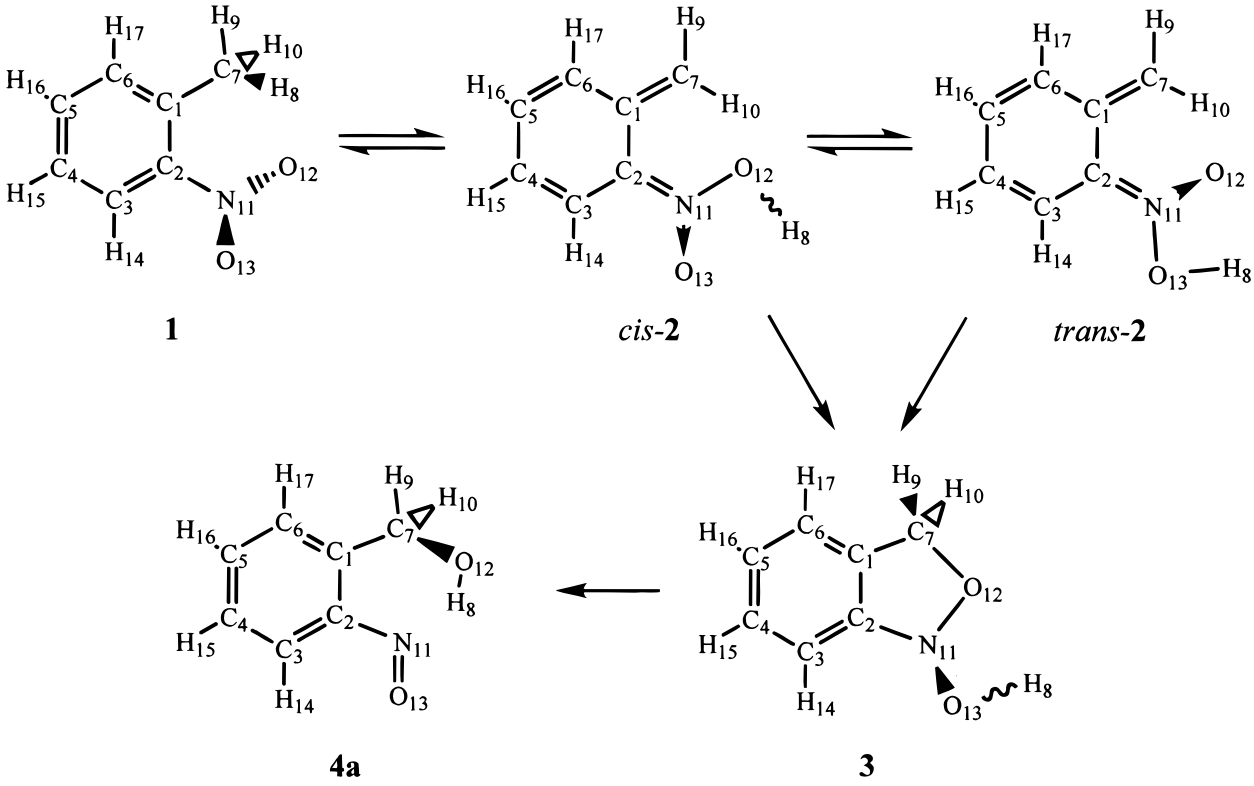

in the form implemented in GAUSSIAN 98. The 6-31G(d) basis set was employed in combination with all three functionals. Four other basis sets, 6-31G(d,p), 6-31+G(d), 6-31G+(d,p), and 6-311+(2d,p), were used in B3LYP calculations. Full geometry optimization for **1**−**3** was also performed at the MP2/6-31G(d) level, where MP2 refers to second-order Møller−Plesset perturbation theory with the frozen core electrons of the heavy atoms. The potential energy surface of **1** and some other molecules was found to be extremely flat near the minimum so that the standard optimization procedure using the approximate Hessian matrix was terminated prior to full convergence. In such cases the final geometry optimization was done by calculation of the force constants at every point.

Finally, single-point energies for the B3LYP geometries were computed at the BHLYP and B3LYP levels of theory with the 6-311+G(2d,p) and 6-311++G(3df,2p) basis sets. For several structures optimized at both the MP2 and B3LYP levels, the quadratic configuration interaction method including corrections for triple substitutions[16] (QCISD(T)) with the 6-31G(d,p) basis set was also employed to obtain single-point energies.

Transition structures (TS) on the potential energy surface were located by using the facility of GAUSSIAN for the synchronous transit-guided quasi-Newton method.[17] The reaction pathways were computed for each TS to verify its connection to the local minima. Reaction paths were calculated by using the "intrinsic reaction coordinate" (IRC) approach[18] as it is implemented in GAUSSIAN 94. For all stationary points the wave function stability was tested and harmonic vibrational frequencies were calculated by using analytical second derivatives.

Results

Structure and Properties of *o*-Nitrotoluene (1). Scheme 2 shows the atom numbering used for **1** and its isomers. The geometry of **1**, optimized at different levels of theory, is given in Tables 1 and 2. Shishkov et al.[19] have recently determined the molecular structure of **1** from electron diffraction data and ab initio calculations. Differences in the C−C bond lengths computed with the MP2(fc)/6-31G(d) method were used as constraints in this structure analysis. The reported bond lengths are distance averages including effects of all vibrations at the experimental temperature (415 K). These quantities should, therefore, be larger than the computed equilibrium bond

TABLE 1: Bond Lengths and Selected Nonbonded Distances of 1 Computed at Different Levels of Theory with the 6-31G(d) (A), 6-31G(d,p) (B), and 6-311+G(2d,p) (C) Basis Sets

		MP2(fc),[b]	A		B3LYP		
	exptl[a]	A	BHLYP	B3PW91	A[b]	B	C
C_1-C_2	1.405	1.403	1.398	1.407	1.410	1.410	1.403
C_1-C_6	1.399[c]	1.403	1.393	1.402	1.404	1.404	1.399
C_1-C_7	1.508	1.506	1.503	1.504	1.510	1.509	1.506
C_2-C_3		1.394	1.387	1.395	1.398	1.398	1.392
C_2-N_{11}	1.490	1.466	1.459	1.469	1.475	1.475	1.475
C_3-C_4		1.392	1.379	1.387	1.389	1.389	1.384
C_3-H_{14}	1.097[c]	1.085	1.074	1.084	1.083	1.082	1.080
C_4-C_5		1.396	1.386	1.394	1.396	1.395	1.391
C_4-H_{15}		1.087	1.077	1.086	1.086	1.085	1.082
C_5-C_6		1.395	1.383	1.391	1.393	1.393	1.388
C_5-H_{16}		1.087	1.078	1.087	1.086	1.086	1.083
C_6-H_{17}		1.088	1.078	1.087	1.087	1.086	1.084
C_7-H_8	1.103[c]	1.092	1.085	1.094	1.093	1.092	1.090
C_7-H_9		1.093	1.085	1.094	1.094	1.093	1.090
C_7-H_{10}		1.092	1.085	1.094	1.094	1.093	1.091
$N_{11}-O_{12}$	1.231	1.244	1.211	1.226	1.232	1.232	1.226
$N_{11}-O_{13}$	1.231	1.244	1.211	1.226	1.232	1.232	1.226
C_7-O_{12}		2.775	2.692	2.711	2.715	2.712	2.752
H_8-O_{12}	2.56	2.556	2.471	2.482	2.486	2.481	2.525
$H_{10}-O_{12}$		2.596	2.510	2.528	2.525	2.519	2.572

[a] Gas-phase electron diffraction data.[19] [b] From ref 19 and this work. [c] An average for all bonds of this type.

TABLE 2: Bond Angles, Selected Nonbonded Angles and Dihedrals (in Degrees) for 1 Computed at Different Levels of Theory with 6-31G(d) (A), 6-31G(d,p) (B), and 6-311+G(2d,p) (C) Basis Sets

					B3LYP		
	exptl[a]	MP2(fc),[b] A	BHLYP, A	B3PW91, A	A[b]	B	C
$C_2-C_1-C_6$	114.8	115.6	115.8	115.7	115.8	115.8	115.8
$C_2-C_1-C_7$	127.3	124.5	125.6	125.5	125.6	125.6	125.3
$C_6-C_1-C_7$		119.9	118.6	118.7	118.6	118.6	118.9
$C_1-C_2-C_3$	124.2	123.5	122.6	122.5	122.5	122.5	122.7
$C_1-C_2-N_{11}$		120.5	121.5	121.6	121.7	121.7	121.4
$C_3-C_2-N_{11}$	113.8	116.0	115.9	115.8	115.8	115.8	116.0
$C_2-C_3-C_4$	118.6	119.0	119.8	119.9	119.9	119.9	119.8
$C_2-C_3-H_{14}$		119.2	118.7	118.5	118.5	118.4	118.7
$C_4-C_3-H_{14}$		121.8	121.5	121.6	121.6	121.7	121.5
$C_3-C_4-C_5$	119.8	119.6	119.2	119.2	119.2	119.2	119.2
$C_3-C_4-H_{15}$		119.8	120.0	120.0	120.0	120.0	120.0
$C_5-C_4-H_{15}$		120.6	120.8	120.8	120.8	120.8	120.8
$C_4-C_5-C_6$	119.6	120.0	120.2	120.1	120.1	120.1	120.2
$C_4-C_5-H_{16}$		120.2	120.2	120.3	120.3	120.2	120.2
$C_6-C_5-H_{16}$		119.8	119.6	119.6	119.7	119.7	119.6
$C_1-C_6-C_5$	123.1	122.3	122.4	122.5	122.5	122.5	122.4
$C_1-C_6-H_{17}$		118.3	118.2	118.1	118.1	118.1	118.2
$C_5-C_6-H_{17}$		119.4	119.4	119.4	119.4	119.4	119.4
$C_1-C_7-H_8$		112.0	111.9	112.1	112.0	111.9	112.1
$C_1-C_7-H_9$		109.3	109.4	109.6	109.5	109.6	109.5
$C_1-C_7-H_{10}$		111.2	111.4	111.4	111.5	111.4	111.2
$H_8-C_7-H_9$		108.5	108.8	108.7	108.8	108.9	108.7
$H_8-C_7-H_{10}$		107.0	106.5	106.2	106.2	106.1	106.4
$H_9-C_7-H_{10}$		108.8	108.8	108.7	108.8	108.9	108.7
$C_2-N_{11}-O_{12}$		117.8	118.4	118.3	118.4	118.4	118.1
$C_2-N_{11}-O_{13}$		117.5	117.7	117.6	117.7	117.7	117.6
$O_{12}-N_{11}-O_{13}$	124.9	124.7	123.9	124.1	123.8	123.8	124.3
$C_1-C_7-O_{12}$		77.0	77.5	77.8	77.9	78.0	77.2
$C_7-H_8-O_{12}$		89.7	89.6	89.9	89.9	90.1	90.1
$C_7-H_{10}-O_{12}$		87.7	87.6	87.6	87.9	88.1	87.6
$C_7-O_{12}-N_{11}$		87.9	94.5	94.0	94.3	94.4	91.5
$C_6-C_1-C_2-C_3$		−0.4	0.0	0.0	0.0	0.0	0.0
$C_6-C_1-C_2-N_{11}$		180.0	180.0	180.0	180.0	180.0	−180.0
$C_7-C_1-C_2-C_3$		179.0	179.1	179.1	179.2	179.3	178.5
$C_7-C_1-C_2-N_{11}$		−0.9	−0.9	−1.0	−0.8	−0.7	−1.4
$C_2-C_1-C_7-H_8$		−44.3	−51.3	−50.5	−51.8	−52.1	−46.9
$C_2-C_1-C_7-H_9$		−164.5	−171.9	−171.3	−172.6	−173.0	−167.6
$C_2-C_1-C_7-H_{10}$		75.4	67.8	68.3	66.9	66.5	72.1
$C_1-C_2-N_{11}-O_{12}$	−38[c]	−34.7	−15.2	−16.1	−13.7	−13.0	−24.8
$C_1-C_2-N_{11}-O_{13}$		146.3	165.3	164.5	166.8	167.4	155.9
$C_2-N_{11}-O_{12}-H_8$		55.4	38.0	38.9	36.3	35.7	46.9

[a] See Table 1. [b] See Table 1. [c] Negative sign was added for purpose of comparison.

lengths,[19,20] but the magnitudes of vibrational corrections are usually less than 0.02 Å.[20]

Generally, all hybrid DFT methods used with the 6-31G(d) basis set yielded much better results for the geometry of **1** as compared to SCF and MP2 calculations. Among the DFT techniques, the B3PW91 bond lengths are in the best agreement with the experimental ones. The B3LYP technique provided a similar value of the root-mean-square error (rms), its main weakness being a noticeable overestimation of the N−O bond lengths. The bond lengths computed with the BHLYP method are substantially shorter than the experimental ones, but the differences are too large to be accounted for by vibrational effects. For the bond angles, the performance of all techniques was found to be similar (rms = 1.3−1.4°). All DFT methods used predicted a minimum-energy structure of **1** with the NO_2 group twisted relative to the benzene ring plane. However, absolute values of the torsion angle were found to be substantially smaller than the experimental one and that predicted with the MP2 method (see Table 2). From the B3LYP/6-31G(d) vibrational analysis we found that a structure with the nitro group lying in the ring plane is a transition structure (TS) with an imaginary frequency of 19.95 cm^{-1} corresponding to the NO_2 torsion. This TS is only 0.02 kcal mol^{-1} above the minimum.

Effects of the basis set on the calculated geometry of **1** were tested for the B3LYP method. There is hardly any difference in the bond lengths predicted with the 6-31G(d), 6-31G(d,p), and 6-31+G(d,p) (not shown) basis sets. In contrast to the 6-31G(d) distances, all bond lengths computed with the 6-311+G(2d,p) basis set are shorter than the experimental ones, all deviations being in the range expected for vibrational corrections. It is worth noting that the 6-311+G(2d,p) bond lengths and angles are in excellent agreement with the corresponding parameters in 2,4,6-trinitrotoluene, which were obtained from X-ray data.[21] Adding diffuse functions on the heavy atoms improved significantly the computed value of the NO_2 torsion angle (13.0° and 20.5° at 6-31G(d,p) and 6-31+G(d,p)). The best value of 24.8° for this angle was obtained with the 6-311+G(2d,p) basis set.

The performance of the selected computational techniques was assessed also by comparing calculated harmonic vibrational frequencies of **1** with the 39 observed fundamentals.[22] The SCF, MP2, BHLYP, B3PW91, and B3LYP frequencies yielded rms values of 174, 98, 124, 72, and 66 cm^{-1}, respectively. By using a single scaling factor for all frequencies we obtained the rms values of 29 (HF), 44 (MP2), 21 (B3PW91), and 19 cm^{-1} (B3LYP). The optimized scaling factors for the selected methods, except BHLYP, have been published previously (0.8953, 0.9434, 0.9573, and 0.9614 for HF, MP2(fc), B3PW91, and B3LYP methods).[23] These results clearly demonstrate better performance of the DFT methods. Not all fundamentals in the

observed spectra of **1** have been identified or assigned. The agreement between calculated and observed frequencies in a simple one-to-one comparison might therefore be accidental. However, linear regression analysis for the whole set of data yielded correlation coefficients $r > 0.998$, the smallest value of 0.9987 being obtained for SCF data. The probability of getting such values by accident, i.e., by using a set of ordered random numbers, is extremely small ($<10^{-6}$).[24]

The dipole moment (μ) of **1** was also taken as a benchmark for the performance of different ab initio and DFT procedures. The experimental values are in the range of 3.8−4.0 D.[25] All methods used with the 6-31G(d) basis set overestimated μ, the largest error being produced by the MP2 method (4.96 D). The best estimates were obtained by using the B3PW91 (4.29 D) and B3LYP techniques (4.33 D). Extension of the basis set did not improve the performance of the B3LYP method ($\mu = 4.30$, 4.37, and 4.49 D for the 6-31G(d,p), 6-31+G(d,p), and 6-311+G(2d,p) basis set, respectively).

Quinonoid Intermediates (2). We located three stationary points corresponding to the *aci*-form **2**. For the cis-isomer we found an anti and a syn-conformer, *cis*-**2a** and *cis*-**2b**. Geometry optimizations for *trans*-**2** started from different points yielded the same minimum corresponding to a syn-conformer. Here, cis and trans indicate the position of the *N*-hydroxyl group relative to the methylene group, anti and syn refer to the OH-group orientation relative to the second oxygen atom. The optimized structures of the quinonoid intermediates are depicted in Figure 1 (Cartesian coordinates for all stationary points are available as Supporting Information), the atom numbering in **2** being shown in Scheme 2.

Compared to **1**, the C_1-C_7, C_2-N, C_3-C_4, and C_5-C_6 bonds become shorter and the four other C−C bonds substantially longer in the *aci*-forms, as implied by the quinonoid valence structure. Computed geometries compare well with available X-ray data for benzoyl and silyl nitronates.[26] The N−O bond lengths (1.250 and 1.418 Å in *trans*-**2**, here and below the B3LYP/6-31G(d,p) geometries are presented unless otherwise stated) are in the range of experimental values (1.232−1.271 and 1.400−1.453 Å). The computed C−N bond lengths (1.333 Å for *trans*-**2**) are slightly larger than the experimental ones of 1.302−1.318 Å. The bond angles predicted for *trans*-**2** are also in reasonable agreement with the experimental values for nitronates (C_1-C_2-N, 120.1° and 121.3−125.2°; C_3-C_2-N, 119.4° and 115.5−118.0°; C_2-N-O_{12}, 129.5° and 129.7−130.3°; C_2-N-O_{13}, 115.7° and 114.0−114.7°; O−N−O, 114.8° and 115.3−116.2° for *trans*-**2** and nitronates, respectively). There is no significant difference in the B3LYP structural parameters of *trans*-**2** computed with the 6-31G(d) and 6-31G(d,p) basis sets. Similar to **1**, extension of the basis set to 6-311+G(2d,p) resulted in slight shortening (<0.006 Å) of all bonds. The MP2/6-31G(d) geometry of *trans*-**2** generally compares well to the DFT results, except that the second-order perturbation theory strongly overestimates the C−N bond length (1.354 Å).

Two isomers *cis*-**2b** and *trans*-**2** are predicted to be completely planar. In contrast, the structure of *cis*-**2a** strongly deviates from planarity. The formally double N═O bond (1.232 Å) in this conformer is noticeably shorter than that in *cis*-**2b** (1.252 Å), while the N−OH bond has practically the same length in both conformers (1.400 and 1.403 Å). Two double bonds outside of the benzene ring are slightly elongated in *cis*-**2a** in comparison to *cis*-**2b**.

All isomers of **2** are substantially destabilized relative to **1** (see Figure 1). The B3LYP energy of the most stable isomer

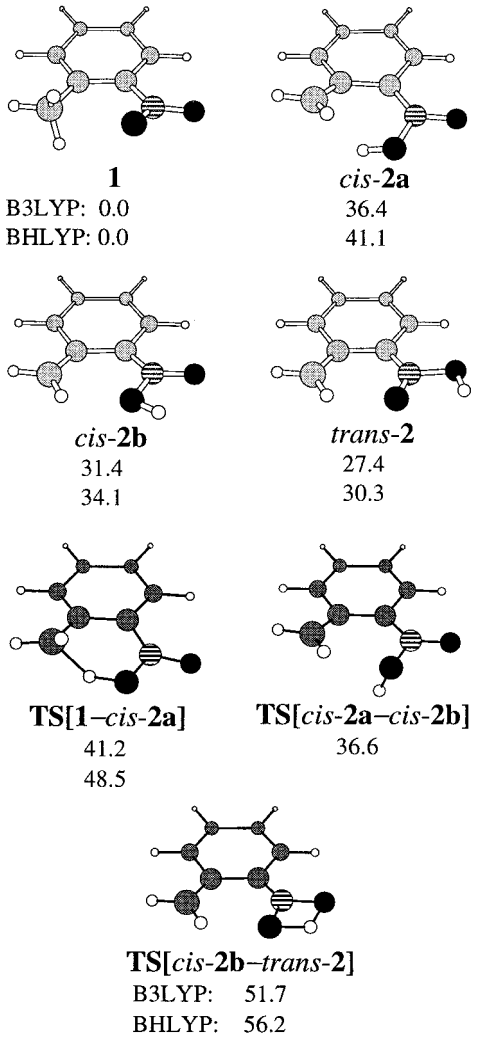

Figure 1. B3LYP/6-31G(d,p) optimized geometries of **1** and **2** and transition structures connecting them. The B3LYP/6-311+G(2d,p)-(+sZPE) and BHLYP/6-311+G(2d,p)(+sZPE) single-point energies computed at these geometries are given in kilocalories per mole relative to the energy of **1**. sZPE refers to the B3LYP/6-31G(d) zero-point vibrational energy scaled by 0.9806. The white circles represent the H atoms, the gray circles the C atoms, the black circles the O atoms, and the circles with horisontal lines the N atoms.

trans-**2** amounts to 27.4 kcal mol^{-1}. Here and below all relative energies were calculated by using the B3LYP/6-311+G(2d,p) or BHLYP/6-311+G(2d,p) single-point energies, which were corrected by the B3LYP/6-31G(d) zero-point vibrational energies scaled by 0.9806.[23b] The BHLYP energy of *trans*-**2** (30.3 kcal mol^{-1}) is close to the energies computed with QCISD(T)/6-31G(d,p) at the B3LYP/6-31G(d) and MP2/6-31G(d) geometries (32.6 and 33.5 kcal mol^{-1}). The difference in the Gibbs free energies of **1** and *trans*-**2** was used to calculate an equilibrium constant K_T for the reaction **1** → *trans*-**2**. The B3LYP free energies gave pK_T of 20.4, which is in reasonable agreement with that of 21.4 calculated as a difference in pK_a of nitrotoluene (25)[27] and its *aci*-form in water (3.6).[9] The BHLYP energies yielded a pK_T value of 22.6.

The TS for a [1,5]H-shift in **1** (see **TS**[**1**−*cis*-**2a**] in Figure 1) was found to be "late", resembling the product *cis*-**2a** with alternating single and double C−C bonds. The C−H bond is broken and the O−H bond is formed to a large extent in this TS (C_7-H_8, 1.516 Å; $O_{12}-H_8$, 1.128 Å). A decrease of 0.71 D in μ was predicted for **TS**[**1**−*cis*-**2a**] compared to **1**. The anti-conformer *cis*-**2a** isomerizes by OH-group rotation into the syn-

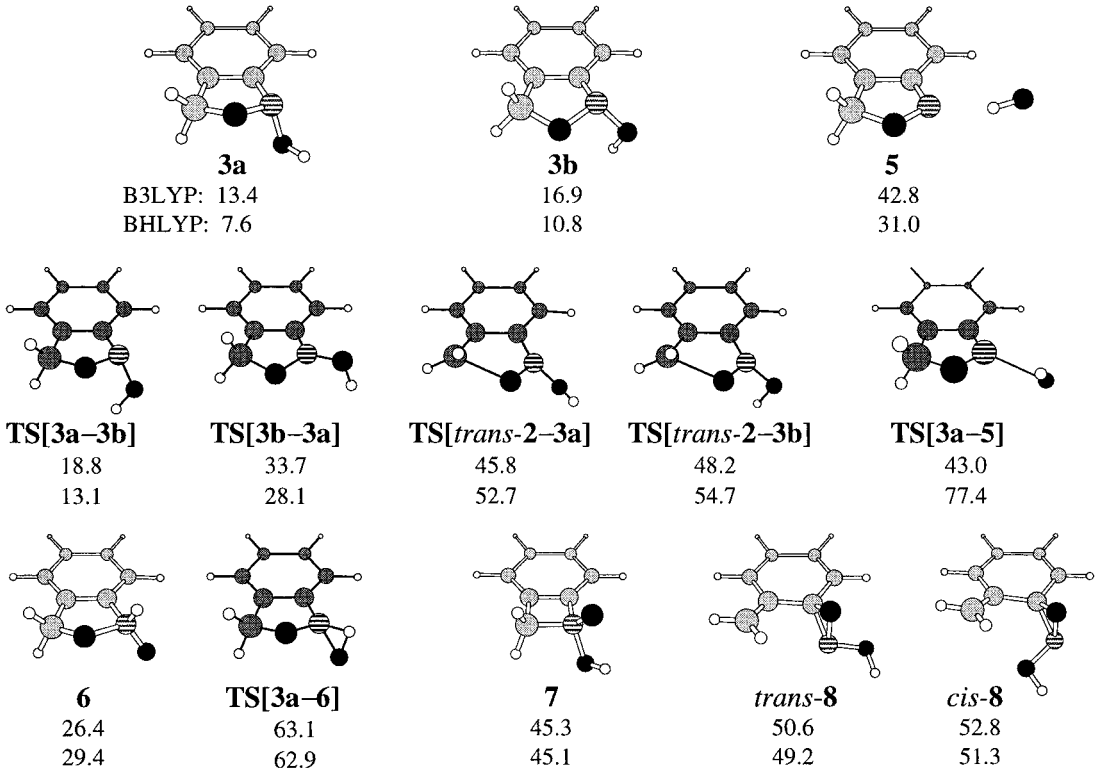

Figure 2. B3LYP/6-31G(d,p) optimized geometries of the bicyclic intermediates **3** and **6** and the transition structures connecting them. The B3LYP/6-31G(d) structures of **5**, **7**, **8**, **TS[3b−3a]**, **TS[3a−5]**, and **TS[*trans*-2−3b]** are also presented. Explanations for the energies are given in Figure 1.

conformer *cis*-**2b** that is 5.0 kcal mol^{-1} (B3LYP) lower in energy. The reaction encounters an activation barrier of 0.2 kcal mol^{-1}, which is substantially smaller than that of 4.7 kcal mol^{-1} for the backward H-transfer. An interesting finding is the diradical character of the TS for the OH rotation in *cis*-**2** (**TS**[*cis*-**2a**−*cis*-**2b**]). Its geometry fully optimized at the UB3LYP/6-31G(d,p) level is depicted in Figure 1. Wave function instability was detected for this TS initially optimized at the RB3LYP/6-31G(d) level. A sizable bond lengthening for all atoms connected to the nitrogen was predicted for **TS**[*cis*-**2a**−*cis*-**2b**] as compared to *cis*-**2b**. This result is in accord with the MP2/6-31G(d) prediction for geometrical parameters of the anti-conformer of *aci*-nitromethane, which was found to be a TS for rotation around the N−OH bond.[28] The barrier for this rotation amounts to 6.8 kcal mol^{-1} at the G1 level. It is worth mentioning that the anti-conformer is a SCF minimum destabilized by 7.7 kcal mol^{-1} (MP2(full)/6-31G(d)//6-31G(d)) relative to the syn-conformer.[29]

The isomerization of *cis*-**2b** to *trans*-**2** may proceed by two mechanisms: a [1,3]H-shift and rotation around the C=N bond. We located a planar transition structure, **TS[***cis*-**2b**−*trans*-**2]**, corresponding to a concerted H-transfer in the *aci*-form. The C−N bond length (1.317 Å) and the O−N−O angle (102.9°) are substantially reduced in this TS in comparison to the quinonoid intermediates. Both N−O bonds were predicted to be of about the same length (1.331 and 1.333 Å) in **TS[***cis*-**2b**−*trans*-**2]** as in the deprotonated *aci*-form **2**$^-$ (see below). This, together with an increase in μ by ca. 1 D (relative to *cis*-**2b**) and a large positive charge on the moving H_8-atom in **TS[***cis*-**2b**−*trans*-**2]**, indicates that the isomerization is best described as an intramolecular proton transfer, in contrast H-atom shift mechanism predicted for the reaction **1** → *cis*-**2a**. A large activation barrier of 20.3 kcal mol^{-1} (B3LYP) was obtained for the reaction *cis*-**2b** → *trans*-**2**. This value can be compared to the hydrogen migration barrier of 27.1 and 26.8 kcal mol^{-1} predicted at QCISD(T) and G2(PU) levels for the almost thermoneutral 1,3-hydrogen shift in HNN(OH)O.[30] For the degenerate [1,3]H-shift in HONO Jursic[31] has obtained an activation barrier of 28.9 and 28.3 kcal mol^{-1} at the CBSQ and B3LYP/6-311G(3df,3pd) levels, respectively. The lower value of the barrier height for *cis*-**2b** may be attributed to the higher exothermicity of the reaction *cis*-**2b** → *trans*-**2** that amounts to 4.0 kcal mol^{-1} (B3LYP). An exothermicity of 3.8 kcal mol^{-1} and an activation energy of 22.1 kcal mol^{-1} were obtained for this reaction with the BHLYP functional.

Bicyclic Intermediates (3). We found two minima with stable restricted wave functions, **3a** and **3b** (see Figure 2), that correspond to the anti and syn conformers of *N*-hydroxy-2,1-benzisoxazoline (**3**). Practically no difference was found in the B3LYP/6-31G(d) and B3LYP/6-31G(d,p) geometries. Shortening by 0.003−006 Å for all bonds except N−O_{13}, flattening of the five-membered ring, and OH group rotation by ca. 3° were obtained upon extension of the basis set to 6-311+G(2d,p). The MP2/6-31G(d) geometry of **3a** is in close agreement with the B3LYP/6-31G(d) result, the largest deviation being a shortening of the C−N bond by 0.008 Å. Second-order perturbation theory also predicted a slightly different configuration of the NOOH group.

In the absence of experimental data on the molecular structure of 2,1-benzisoxazolines, we compare the B3LYP/6-31G(d,p) structure of **3a** with gas-phase data for NH_2OH[32] and X-ray data for *N*-methoxy isoxazolidines.[33,34] Excellent agreement between the experimental parameters for hydroxylamine and the calculated ones for **3a** (N−O−H, 101.4° and 101.5°; N−O, 1.453 and 1.451 Å; O−H, 0.962 and 0.969 Å, in NH_2OH and **3a**, respectively) was found. The geometry of **3a** is also in reasonably good agreement with experimental data for isoxazolidines (C_1−C_7, 1.502 and 1.50−1.53 Å; N−O_{12}, 1.434 and

1.41−1.43 Å; N−O_{13}, 1.451 and 1.43−1.47 Å; C_7−O_{12}, 1.446 and 1.45−1.46 Å for **3a** and isoxazolidines, respectively). However, the C_2−N bond (1.441 Å) in **3a** is noticeably shorter than that in these compounds (1.48−1.50 Å). This shortening may be attributed to stronger coupling between the nitrogen and the carbon located within the benzene ring in **3a**. An envelope-like conformation of **3a** with the oxygen atom out of the molecular plane resembles the conformation of fused isoxazolidines determined by NMR spectroscopy and X-ray analysis.[33b]

The structure of the syn-conformer **3b** differs noticeably from that of **3a**. The five-membered ring in **3b** adopts a conformation with a pseudoequatorial position of the OH group. An OH···O hydrogen bond may be responsible for the stabilization of this conformation. The H_8−O_{12} distance was found to be smaller in **3b** (2.390 Å) than in **3a** (2.674 Å). Substantial lengthening of the endo N−O_{12} bond (1.475 Å) and shortening of the N−O_{13} (1.398 Å) and C_7−O_{12} (1.437 Å) bonds were predicted for **3b**. The anti-conformer **3a** is destabilized by 13.4 kcal mol^{-1} relative to **1** at the B3LYP level. This energy difference reduces to 7.6 kcal mol^{-1} at the BHLYP level of theory.

The interconversion of the two conformers of **3** can be considered in terms of two different mechanisms: rotation around the exo N−O bond or nitrogen inversion. In both cases the primary process should be accompanied by conformational change of the isoxazoline ring, i.e., rotation around the endo N−O bond. We found transition structures for both mechanisms (Figure 2). At the B3LYP level the isomerization of **3b** to **3a** is thermodynamically favorable by 3.5 kcal mol^{-1} and has an activation barrier of 1.9 and 16.8 kcal mol^{-1} for the OH rotation and nitrogen inversion, respectively. These parameters changed only slightly (<0.4 kcal mol^{-1}) when the BHLYP energies were used. The N−OH bond rotation barrier in **3b** compares reasonably well to that in NH_2OH, which amounts to 2.72 kcal mol^{-1} at the G2 level[35a] and 2.1 kcal mol^{-1} at the CCSD(T)/6-311++G(d,p) and B3LYP/6-311++G(d,p) levels.[35b]

At the UB3LYP/6-31G(d) level we were able to locate a minimum-energy structure (**5** in Figure 2) corresponding to a radical pair formed upon the N−OH bond fission in **3a**. The UB3LYP/6-31G(d) geometry of a diradical TS connecting **3a** to **5** (**TS[3a−5]**) is very close to that of the product except for the position and orientation of the OH group. The reaction **3a** → **5** was predicted to be endothermic by 29.4 kcal mol^{-1} and to have an activation barrier of 29.6 kcal mol^{-1}at the UB3LYP/6-311+G(2d,p) level. The former value compares well to the G2(PU/B3LYP) energy of 31.5 kcal mol^{-1} for the OH elimination from HN(O)OH.[36] By using the UBHLYP method we obtained a reaction endothermicity of 23.4 kcal mol^{-1} and a barrier height of 69.8 kcal mol^{-1}.

Three other bicyclic isomers (see **6**−**8** in Figure 2) of 2-nitrotoluene were found in our DFT study. The most important features distinguishing the geometry of the nitrone **6** from that of **3a** are the N−X bond lengths (C−N, 1.472 Å; N−O_{12}, 1.732 Å; N−O_{13}, 1.250 Å). The molecular structure of the TS (**TS-[3a−6]**) corresponding to a [1,2]H-shift in **3a** is shown in Figure 2. A shorter C−N bond (1.434 Å) and elongated N−O bonds (N−O_{12}, 1.448 Å; N−O_{13}, 1.460 Å) were predicted for **TS-[3a−6]** as compared to **3a**. The N−H distance (1.112 Å) in **TS[3a−6]** was found to be smaller than the O−H one (1.313 Å). This result is in accord with the computed geometry of a TS corresponding to a 1,2-hydrogen shift in structurally related formaldoxime.[37] An endothermicity of 13.0 kcal mol^{-1} and an activation barrier of 49.7 kcal mol^{-1} were predicted for the reaction **3a** → **6** at the B3LYP level. The BHLYP technique yielded reaction and activation energies of 21.8 and 55.3 kcal mol^{-1}, respectively. The latter value is close to the activation energy of 54.4 kcal mol^{-1} for the [1,2]H-shift in formaldoxime as computed at B3LYP/6-311G(d,p).[37b] Two other bicyclic isomers, **7** and **8**, were found to be substantially higher in energy than **3** and **6** (see Figure 2). They do not appear to play a significant role in the transformations considered here.

We explored several possible ways for the formation of **3** from the *aci*-forms. Although direct cyclization of *cis*-**2b** seems to be unfavorable, at the RB3LYP/6-31G(d) level we were able to locate a TS (see **TS[***cis*-**2b**−**3a]** in the Supporting Information) that, according to IRC calculations, connects *cis*-**2b** with **3a**. However, wave function instability was detected for this TS. Our attempts to locate another singlet diradical TS failed. These results suggest that a more favorable pathway for the *cis*-**2b** cyclization may exist in the triplet manifold.

Two transition structures, (see **TS[***trans*-**2**−**3a]** and **TS[***trans*-**2**−**3b]** in Figure 2), were found for the cyclization of *trans*-**2**. Both TS are structurally similar, except for the orientation of the OH group. All double bonds and both N−O bonds are elongated and the single C−C bonds are shortened in these transition structures as compared to *trans*-**2**. Pronounced changes in the configuration of the CH_2 and NOOH groups corresponding to an sp^2-to-sp^3 hybridization change were predicted for both TSs. There is no significant difference (<0.006 Å in bond lengths, < 0.9° in angles) in the B3LYP geometries of **TS-[***trans*-**2**−**3a]** optimized with the 6-31G(d), 6-31G(d,p), and 6-311+G(2d,p) basis sets. The MP2/6-31G(d) geometry of **TS-[***trans*-**2**−**3a]** is generally close to the B3LYP/6-31G(d) result. The largest differences were found in the C_7−O_{12} (2.158 and 2.116 Å at B3LYP and MP2 level) and N−O_{12} distances (1.278 and 1.264 Å). For the angles, the largest deviations of MP2 results were increases in the H_{10}−C_7−O_{12}, C_2−C_1−C_7−H_{10}, and C_1−C_2−N−O_{13} angles by 3.9°, 7.7°, and 7.1°, respectively.

Exothermicity of 14.0 kcal mol^{-1} and an activation barrier of 18.4 kcal mol^{-1} were predicted for the cyclization *trans*-**2** → **3a** at the B3LYP/6-311+G(2d,p)//B3LYP/6-31G(d,p) level. These parameters increase only by 0.04 and 0.05 kcal mol^{-1}, respectively, for the B3LYP/6-311+G(2d,p) geometries. By computing the B3LYP/6-311++G(3df,2p) single-point energies at the latter geometries we obtained additional small increases of 0.10 and 0.24 kcal mol^{-1} in the exothermicity and activation energy. The QCISD(T)/6-31G(d,p) energies computed at the B3LYP and MP2/6-31G(d) geometries yielded slightly smaller values of 17.4 and 17.5 kcal mol^{-1} for the activation energy of this reaction. A higher activation barrier (20.8 kcal mol^{-1} at B3LYP level) for the cyclization *trans*-**2** → **3b** correlates with lower exothermicity (10.5 kcal/mol) of this reaction in comparison to *trans*-**2** → **3a**. A slight increase in the dipole moment is expected when one goes along the reaction coordinate from *trans*-**2** to **3a** (μ = 1.35, 1.57, and 1.51 D for *trans*-**2**, **TS[***trans*-**2**−**3a]**, and **3a**, respectively, at the B3LYP/6-31G(d) level). On the other hand, rather strong polarization in the course of the cyclization leading to **3b** was predicted (μ = 3.53 and 3.77 D for **TS[***trans*-**2**−**3b]** and **3b**).

Nitrosobenzyl Alcohol (4). The conformational surface of **4** was initially explored at the HF/6-31G(d) level. Nine conformers **4a**−**i** (Figure 3) were found. In all structures the nitroso group is only slightly twisted out of the benzene ring plane. Eight conformers can be divided into structurally related couples that have similar configurations of the hydroxymethyl group and differ in the NO-group orientation. We could not locate a stationary point for a conformer that is structurally

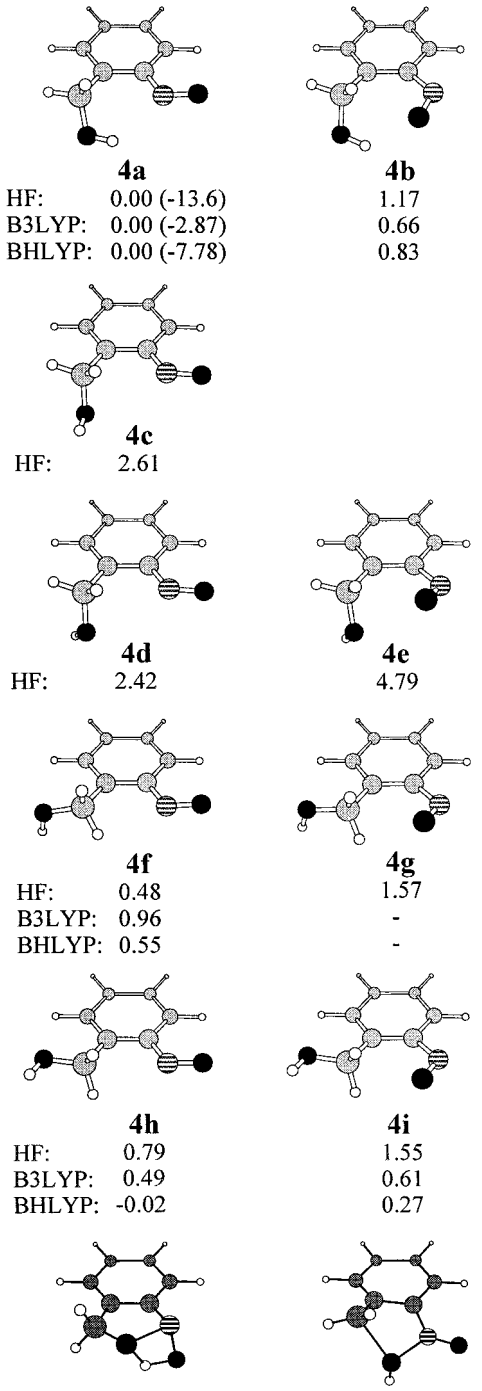

Figure 3. 2-Nitrosobenzyl alcohol conformers **4a**−**i** optimized at the HF/6-31G(d) level. The B3LYP/6-31G(d,p) optimized geometries of the transition structures connecting *cis*-**2b** to **4a** and **3b** to **4b** are also shown. The 6-31G(d)//6-31G(d) energies and the B3LYP/6-311+G(2d,p)(+sZPE) and BHLYP/6-311+G(2d,p)(+sZPE) single-point energies computed at the B3LYP/6-31G(d) geometries are given in kilocalories per mole relative to the energy of **4a**. The energies of the transition structures and **4a** (values in brackets) are also given relative to that of **1**.

related to **4c** and has the nitroso group oriented toward the CH_2OH group.

The five conformers of lowest energy were selected for the B3LYP/6-31G(d) geometry optimization. Finally, **4a**, **4b**, and **4h** were reoptimized at the B3LYP/6-31G(d,p) level. The

TABLE 3: Gas-Phase Deprotonation Enthalpies (kcal mol^{-1}) at 298.15 K and Acidity Constants in Water

reaction	B3LYP/6-311+G(2d,p)// B3LYP/6-311+G(2d,p)	BHLYP/6-311+G(2d,p)// B3LYP/6-311+G(2d,p)	pK_a
1 → **2**$^-$	351.4	357.3	25[a]
cis-**2b** → **2**$^-$	319.8[b]	322.0[b]	
trans-**2** → **2**$^-$	323.9	326.7	3.6[c]
3a → **3**$^-$	347.0	358.1	
6 → **3**$^-$	333.8[b]	335.5[b]	
4b → **4**$^-$	357.0[b]	364.2[b]	

[a] From ref 27. [b] Geometry of the protonated species optimized at the B3LYP/6-31G(d,p) level. [c] From ref 9.

B3LYP/6-31G(d,p) structural parameters of **4h** (C_2−N, 1.434 Å; N−O_{13}, 1.225 Å; C_1−C_2−N, 115.7°; C_2−N−O_{13}, 115.5°) compare well with available experimental data for nitroso compounds in the gas phase (C−N: 1.44−1.48 Å; N═O: 1.21−1.22 Å; C−C−N: 117°; C−N═O: 113−116°).[38−40]

As expected, all conformers with closely spaced nitroso and hydroxymethyl groups are destabilized in comparison to their analogues with two groups oriented into opposite directions. The formation of **4a** from **1** was predicted to be exothermic by 2.9 and 7.8 kcal mol^{-1} at the B3LYP and BHLYP level, respectively. **4b** is destabilized by 0.7−0.8 kcal mol^{-1} relative to **4a** (see also energies in Figures 3 and 6).

In exploring reaction pathways for the formation of **4** directly from the *aci*-form we located a TS with a stable RB3LYP/6-31G(d) wave function that corresponds to an intramolecular transfer of the OH group in cis-**2** (see **TS[***cis*-**2b**−**4a]** in Figure 3). This TS is characterized by weak bonding of the OH group (C_7−O_{12}, 2.075 Å; N−O_{12}, 1.876 Å) and by a large negative charge on the migrating group. A high activation barrier of 39.1 kcal mol^{-1} (B3LYP) was predicted for the reaction *cis*-**2b** → **4a**.

More favorable pathways to **4** were located starting from the bicyclic intermediates **3** and **6**. Figure 3 shows the B3LYP/6-31G(d,p) geometry of a TS for the isomerization **3b** → **4b** via a 1,3-hydrogen shift. The moving hydrogen in **TS[3b**−**4b]** is 1.212 and 1.254 Å apart from the O_{12} and O_{13} atoms, respectively. The exocyclic N−O_{13} bond (1.336 Å) is substantially shortened and the endo N−O_{12} bond (1.852 Å) is practically broken in this TS. The reaction **3b** → **4b** was found to be exothermic by 19.1 and 17.8 kcal mol^{-1} at the B3LYP and BHLYP level, respectively. An activation barrier of 33.4 and 43.0 kcal mol^{-1} was predicted for this reaction by using the B3LYP and BHLYP functionals. At the RB3LYP/6-31G(d) level we also located a TS (see **TS[6**−**4a]** in the Supporting Information) connecting **6** and **4a**. However, wave function instability was detected for this TS, whose energy is only 3.2 kcal mol^{-1} higher than that of **6**. Our attempts to locate another singlet TS with a stable unrestricted wave function failed.

Other Isomers of 2-Nitrotoluene. Formation of 2-aminobenzoic (anthranilic) acid and 2,1-benzisoxazole (anthranil) in thermal reactions of **1** and its derivatives has been reported.[41−47] To obtain energies comparable to those of the other molecules studied, hydrogen-bonded complexes of anthranil with a single water molecule were explored. The B3LYP/6-31G(d) structures of two such complexes, **9a** and **9b**, are depicted in Figure 4. Both of them are strongly stabilized relative to **1** and **4** (see Table 4 and Figure 4). Higher stability of **9b** in comparison to **9a** may be attributed to stronger hydrogen bonding, which is manifested in the shorter H-bond (N···H, 2.032 Å in **9b**; O···H, 2.212 Å in **9a**).

To our knowledge 2-(hydroxylamino)benzaldehyde (**10**) has never been obtained or trapped in reactions of 2-nitrobenzyl

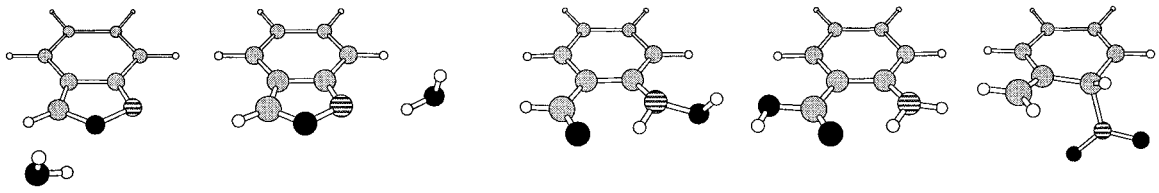

	9a	**9b**	**10**	**11**	**12**
B3LYP:	-22.2	-23.8	-23.8	-81.3	33.0
BHLYP:	-24.8	-26.5	-29.6	-90.0	34.1

Figure 4. B3LYP/6-31G(d) optimized geometries of **9**−**12**. Explanations for the energies are given in Figure 1.

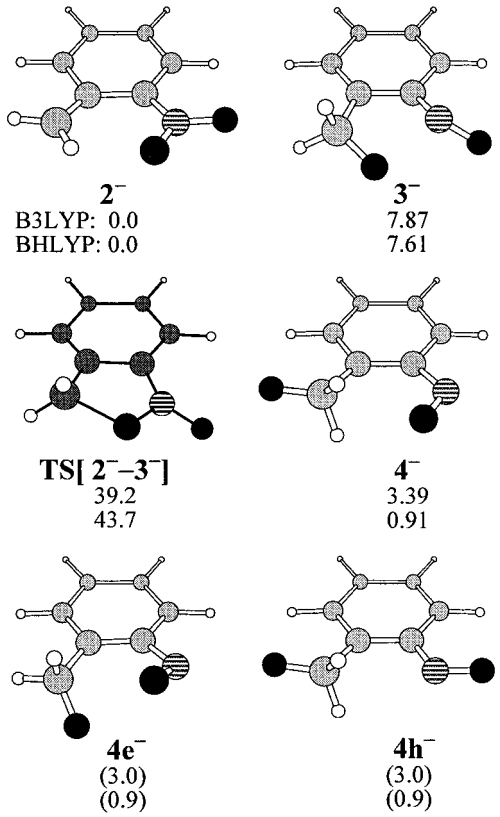

Figure 5. B3LYP/6-311+G(2d,p) optimized geometries of anionic species **2**$^-$−**4**$^-$ and the transition state **TS[2**$^-$−**3**$^-$**]**. The B3LYP/6-311+G(2d,p)(+sZPE) and BHLYP/6-311+G(2d,p)(+sZPE) energies are given in kilocalories per mole relative to the energy of **2**$^-$. sZPE refers to the B3LYP/6-31+G(d) zero-point vibrational energy scaled by 0.9806.

derivatives. Nevertheless, this compounds seems to be a feasible intermediate in the isomerization of nitroso compounds such as **4**. The B3LYP/6-31G(d) structure of a particular conformer of **10** is illustrated in Figure 4. At the B3LYP/6-311+G(2d,p) level this molecule is stabilized by 20.9 kcal mol^{-1} relative to **4a**, the best estimate with the BHLYP method being 21.8 kcal mol^{-1}. Failure to detect **10** experimentally may be due to its high reactivity. Our computational study showed that additional strong stabilization can be reached upon conversion of **10** to anthranilic acid (**11**). At the B3LYP level the reaction **10** → **11** is exothermic by 57.5 kcal mol^{-1}, a value of 60.4 kcal mol^{-1} being found at the BHLYP level.

Figure 4 also shows the B3LYP/6-31G(d) structure of the nonaromatic nitro compound **12** that might be formed via a [1,3]H-shift in **1** or **2**. Although the energy of **12** was predicted to be close to that of the *aci*-form, its formation can hardly compete with other rearrangements because of very high activation barriers characteristic for [1,3]H-shifts involving carbon atoms.[37]

Anionic Species. We performed full geometry optimization at the B3LYP/6-31+G(d) and B3LYP/6-311+G(2d,p) levels for anionic species produced by deprotonation of the molecules **1**−**4**. The geometry of the neutral species without proton H_8 was used as an initial guess for the anion structure. The multitude of local minima found for neutral isomers of **1** reduces substantially for the anionic species. In the ground state we were able to localize only three minima with stable restricted wave functions. The same minimum, **2**$^-$ (Figure 5), was reached in geometry optimizations for anions produced from **1**, *cis*-**2**, *trans*-**2**, and **7**. Deprotonation of these molecules was accompanied by substantial changes in geometry, those for **2** being the smallest. The C−N bond, two almost equal N−O bonds, and the O−N−O angle predicted for **2**$^-$ are quite different from those for *trans*-**2** (C_2−N, 1.398 and 1.327 Å; N−O_{12}, 1.257 and 1.246 Å; N−O_{13}, 1.267 and 1.419 Å; O−N−O, 120.5 and 114.9° in **2**$^-$ and *trans*-**2**, respectively; here and below the B3LYP/6-311+G(2d,p) geometries are presented, unless otherwise stated).

B3LYP geometry optimizations starting from deprotonated **3a**, **3b**, and **6** yielded the same anion **3**$^-$ (Figure 5), which shows surprisingly little similarity with the parent compounds. Rather, it might be considered as a particular conformer of the nitrosobenzyl alcohol anion. We were not able to obtain this structure starting from any stable conformer of **4**, but it was reached in an optimization run started from a hypothetical deprotonated conformer of **4** with properly aligned CH_2O^- and NO groups. The endocyclic N−O_{12} bond was found to be practically broken in **3**$^-$ (N−O_{12}, 2.104 and 1.431 Å in **3**$^-$ and **3a**). In contrast, the N−O_{13} and C_7−O_{12} bonds became much shorter in the anion in comparison to the protonated form (N−O_{13}, 1.243 and 1.450 Å; C_7−O_{12}, 1.365 and 1.448 Å in **3**$^-$ and **3a**, respectively). To test the reliability of the B3LYP prediction for this structure we also performed full geometry optimization at the MP2/6-31+G(d) level starting from the MP2/6-31G(d) geometry of **3a** without H_8. Although the MP2 value of the N−O_{12} bond length (1.942 Å) is noticeably smaller than the B3LYP/6-31+G(d) one (2.099 Å), the rupture of the endocyclic N−O bond in **3**$^-$ is confirmed.

In exploring the conformational surface of the deprotonated form of **4** at the HF/6-31G(d) level we were able to locate only three minima. A common anion **4**$^-$ was found for the conformers **4b**, **4g**, and **4i**. The optimization started from the deprotonated **4e** resulted in an anion **4e**$^-$ that is structurally similar to the parent molecule. Five other conformers **4a**, **4c**, **4d**, **4f**, and **4h** gave anion **4h**$^-$, which is structurally close to **4h**. The geometry of these three anions was reoptimized at the RB3LYP/6-31G(d) level of theory. Surprisingly enough, all minima located at this level were shown to have unstable wave functions. However, stable minima for **4**$^-$ (Figure 5) were

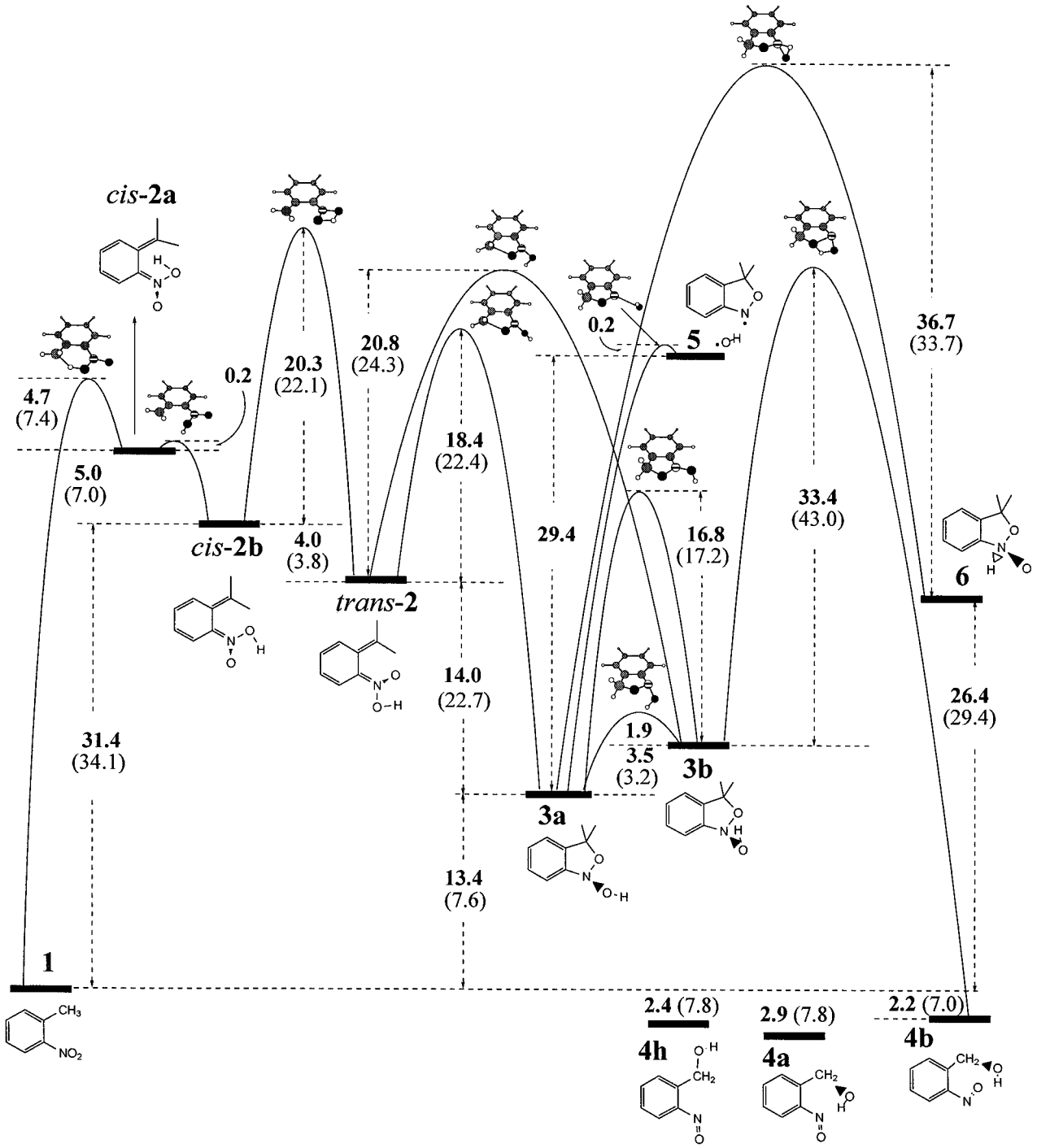

Figure 6. Overall profile of the potential energy surface for the isomerization of 2-nitrotoluene to 2-nitrosobenzyl alcohol calculated at the B3LYP/6-311+G(2d,p)(+sZPE)//B3LYP/6-31G(d,p) level of theory. The geometries of **5**, **TS[3b−3a]**, **TS[3a−5]**, and **TS[*trans*-2−3b]** were optimized at the B3LYP/6-31G(d) level. Values in parentheses were obtained from the BHLYP(+sZPE)/6-311+G(2d,p) single-point energies computed at the same geometries. sZPE refers to the B3LYP/6-31G(d) zero-point vibrational energies scaled by 0.9806.

located in RB3LYP optimization runs using larger basis sets with diffuse functions (6-31+G(d) or 6-311+G(2d,p)). For two other anions in the singlet state we could not locate stable minima at both the R and UB3LYP levels with various basis sets. By performing UB3LYP/6-31G(d) geometry optimization we demonstrated that the lowest triplet states of $\mathbf{4e}^-$ and $\mathbf{4h}^-$ are only 3−5 kcal mol^{-1} above the singlet states. In such a case the single-determinant technique used in this study may be not adequate.

A transition structure connecting $\mathbf{2}^-$ and $\mathbf{3}^-$ was fully optimized at the B3LYP level using the 6-31+G(d) and 6-311+G(2d,p) basis sets. Its best geometry (**TS[$\mathbf{2}^-$−$\mathbf{3}^-$]**) is depicted in Figure 5. Substantial lengthening the N−O_{12} bond in this TS (1.368 Å) in comparison to $\mathbf{2}^-$ (1.257 Å) was predicted. The length of this bond was found to increase from 1.246 Å in *trans*-**2** to 1.278 Å in the neutral **TS[*trans*-2−3a]**.

From the B3LYP and BHLYP energies computed at the B3LYP/6-311+G(2d,p) geometries we obtained similar values of 7.9 and 7.6 kcal mol^{-1} for the endothermicity of the reaction $\mathbf{2}^- \rightarrow \mathbf{3}^-$. However, the activation barrier for this reaction was found to be significantly higher at the BHLYP level (43.7 kcal mol^{-1}) than at the B3LYP one (39.2 kcal mol^{-1}). The latter

TABLE 4: Total Energies (atomic units) of 1−12 and Transition Structures Computed with Different Methods Using the 6-31G(d) (A), 6-31G(d,p) (B), and 6-311+G(2d,p) (C) Basis Sets

molecule	B3LYP/A// B3LYP/A	B3LYP/C// B3LYP/A	BHLYP/C// B3LYP/A	B3LYP/C// B3LYP/B	BHLYP/C// B3LYP/B	ZPE [a]
1	−476.064 987	−476.211 758	−475.915 094	−476.211 766	−475.915 145	82.57
cis-**2a**	−475.996 951	−476.152 231	−475.847 935	−476.152 296	−475.848 185	81.64
cis-**2b**	−476.005 728	−476.161 210	−475.859 118	−476.160 354	−475.859 386	81.69
trans-**2**	−476.010 535	−476.166 316	−475.865 032	−476.166 606	−475.865 284	81.60
3a	−476.038 147	−476.190 464	−475.902 829	−476.190 520	−475.903 030	82.61
3b	−476.032 855	−476.184 719	−475.897 532	−476.184 765	−475.897 741	82.48
4a	−476.062 980	−476.215 928	−475.926 944	−476.215 919	−475.927 119	82.30
4b	−476.061 989	−476.215 003	−475.925 740	−476.214 980	−475.925 919	82.38
4f	−476.060 656	−476.213 788	−475.925 460			81.91
4h	−476.059 443	−476.214 176	−475.926 006	−476.214 224	−475.926 199	81.68
4i	−476.059 742	−476.214 208	−475.925 772			81.82
5[b]	−475.987 405	−476.138 987	−475.767 743			79.69
6	−476.016 327	−476.169 838	−475.869 096	−476.170 322	−475.868 948	83.00
7	−475.981 128	−476.138 096	−475.841 631			81.58
trans-**8**	−475.975 146	−476.127 908	−475.833 582			80.55
cis-**8**	−475.972 067	−476.124 440	−475.830 189			80.52
9a	−476.083 124	−476.244 479	−475.952 099			80.92
9b	−476.087 712	−476.248 011	−475.955 516			81.47
10	−476.093 055	−476.249 683	−475.962 262			82.54
11	−476.182 514	−476.342 372	−476.059 578			83.29
12	−476.006 901	−476.157 821	−475.859 392			81.69
TS[1−*cis*-2a]	−475.988 386	−476.141 003	−475.832 433	−476.140 957	−475.832 684	79.23
TS[*cis*-2a−*cis*-2b][b]	−475.994 554	−476.149 706	−475.845 207	−476.149 690	−475.855 609	80.20
TS[*cis*-2b−*trans*-2]	−475.968 639	−476.123 647	−475.819 399	−476.123 695	−475.819 828	78.90
TS[*cis*-2b−4a]	−475.938 533	−476.095 025	−475.772 895			79.76
TS[*trans*-2−3a]	−475.980 696	−476.136 032	−475.828 158	−476.136 084	−475.828 431	80.81
TS[*trans*-2−3b]	−475.976 692	−476.131 490	−475.824 442			80.35
TS[3a−3b]	−476.028 010	−476.180 633	−475.892 804	−476.180 630	−475.893 013	81.77
TS[3b−3a]	−476.005 010	−476.157 380	−475.869 630			82.12
TS[3a−5][b]	−475.984 036	−476.137 703	−475.786 105			79.00
TS[3a−6]	−475.949 898	−476.106 651	−475.810 079	−476.106 772	−475.810 346	79.68
TS[3b−4b]	−475.973 551	−476.125 205	−475.822 300	−476.125 250	−475.823 044	78.50

[a] Unscaled B3LYP/6-31G(d) zero-point vibrational energy. [b] Geometry optimized at the UB3LYP level.

TABLE 5: Total Energies (atomic units) of Anions 2⁻−4⁻, Neutral Species 1, *trans*-2, and 3a and Transition Structures Connecting Them, Which Were Computed with Different Methods Using the 6-31G(d) (A), 6-31G(d,p) (B), 6-311+G(2d,p) (C), 6-31+G(d) (D), and 6-311++G(3df,2p) (E) Basis Sets

	B3LYP/D// B3LYP/D	B3LYP/C// B3LYP/D	BHLYP/C// B3LYP/D	B3LYP/C// B3LYP/C	B3LYP/E// B3LYP/C	BHLYP/C// B3LYP/C	ZPE [a]
2⁻	−475.511 145	−475.637 880	−475.331 501	−475.638 223	−475.658 118	−475.333 615	73.21
3⁻	−475.499 424	−475.624 059	−475.318 207	−475.624 408	*b*	−475.320 214	72.39
4⁻	−475.505 502	−475.630 158	−475.327 699	−475.630 491	*b*	−475.329 840	71.72
TS[2−3⁻]	−475.448 036	−475.573 171	−475.260 078	−475.573 624	−475.593 022	−475.261 847	71.85
	QCISD(T)/B// B3LYP/A	QCISD(T)/B// MP2/A		B3LYP/C// B3LYP/C	B3LYP/E// B3LYP/C	BHLYP/C// B3LYP/C	
1	−474.792 668	−474.793 335		−476.212 126	−476.232 272	−475.916 864	
trans-**2**	−474.739 168	−474.738 445		−476.166 837	−476.187 142	−475.866 689	
3a				−476.190 748	−476.211 201	−475.904 250	
TS[*trans*-2−3a]	−474.710 270	−474.709 316		−476.136 247	−476.156 164	−475.829 806	

[a] Unscaled B3LYP/6-31+G(d) zero-point vibrational energy. [b] Convergence failed.

value was reproduced within 0.3 kcal mol^{-1} by computing the B3LYP/6-311++G(3df,2p) energies at the same geometries. Stabilization by 4.5 (B3LYP) and 6.7 kcal mol^{-1} (BHLYP) was predicted for the conversion of **3**$^-$ to **4**$^-$.

Table 3 shows calculated gas-phase acidities of several molecules studied in this work. The acidities were calculated as a difference between thermal enthalpies of the anion and the conjugated acid plus the translational enthalpy of a free proton ($3RT/2 = 0.889$ kcal mol^{-1}). The B3LYP and BHLYP methods provided qualitatively consistent pictures for the energetics of the deprotonation reactions. Both stereoisomers of the *aci*-form were predicted to be much stronger acids than the parent compound **1**. The trans-isomer was found to be a weaker acid than the cis-isomer *cis*-**2b** ($\Delta pK_a = 3.0$ and 3.4 at the B3LYP and BHLYP levels, respectively). The benzisoxazoline **3a** is expected to be a much weaker acid than *trans*-**2**, the B3LYP estimate for the gas-phase ΔpK_a being 17.0. Taking into account the comparable dipole moments of **2** and **3**, their relative acidities should not drastically change in aqueous solution. The isomerization of the anion **2**$^-$ at neutral pH may therefore be accompanied by the protonation of the product **3**$^-$. The weakest acid in the gas phase was found to be 2-nitrobenzyl alcohol.

Reaction Profile. The total energies of all stationary points found in this study are presented in Tables 4 and 5. By using the best estimates for the energies we constructed potential energy profiles for the isomerization of the neutral (Figure 6) and anionic forms of **1** (Figure 7). An important finding of this study is the fact that these profiles differ substantially (see Discussion).

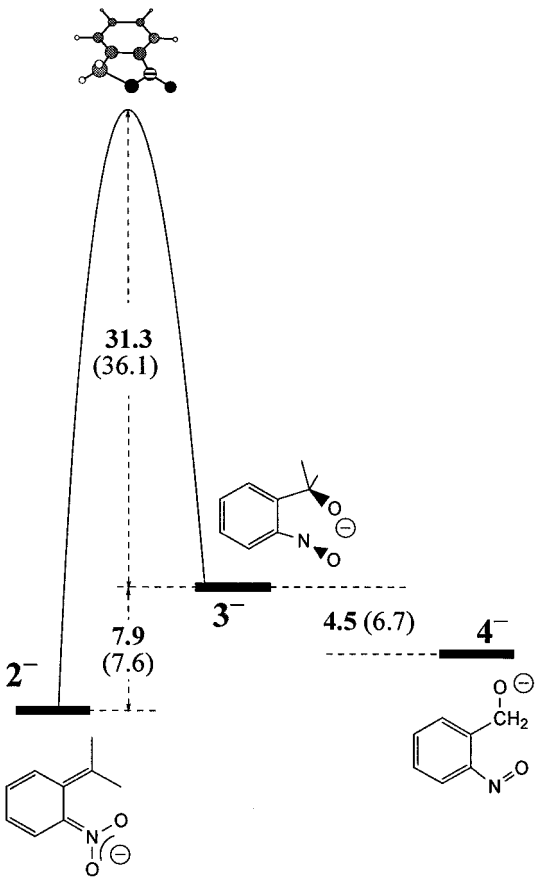

Figure 7. Overall profile of the potential energy surface for the isomerization of 2-nitrotoluene anion to 2-nitrosobenzyl alcohol anion calculated at the B3LYP/6-311+G(2d,p)(+sZPE)// B3LYP/6-311+G-(2d,p) level of theory. Values in parentheses were obtained from the BHLYP(+sZPE)/6-311+G(2d,p) single-point energies computed at the same geometries. sZPE refers to the B3LYP/6-31+G(d) zero-point vibrational energies scaled by 0.9806.

Discussion

Photochemical and Thermal Reactions of Nitrobenzyl Compounds. The primary photoreaction of 2-nitrotoluene (**1**),[9,48−51] polynitrotoluenes,[49−56] and 2-nitrobenzyl derivatives[44,49,51,56−61] is an intramolecular 1,5-hydrogen shift, which occurs on the subnanosecond time scale and affords the *aci*-form of the nitro compounds. These quinonoid intermediates are easily detected by nanosecond flash photolysis due to their strong absorption around 400 nm. The *aci*-forms are much stronger acids than the parent nitro tautomers.[49,62] Protolytic equilibria involving quinonoid intermediates may therefore play an essential role in the mechanism and kinetics of the photoinduced reaction of nitrobenzyl derivatives.

Trentham and co-workers[60,61] studied the photoinduced reaction of 2-nitrobenzyl phosphate esters in aqueous solutions at pH close to 7. The *aci*-nitro anion was found to be formed upon fast deprotonation of the quinonoid intermediate, which is produced in the photoreaction of a nitrobenzyl precursor. The rate of the anion decay was shown to be equal to that of the *o*-nitroso compound formation and of phosphate release. The reaction was assumed to proceed through a benzisoxazoline intermediate being in fast equilibrium with the *aci*-nitro anion, Scheme 3.[60] Our work indicates that this equilibrium cannot be established, and that, depending on pH, the *aci*-form cyclization may or may not be rate-limiting for the release of anions from nitrobenzyl cages (vide infra). Moreover, nonexponential decay of the 400-nm transient absorption has been noted in several

SCHEME 3: Mechanism of the Photoinduced Isomerization of 2-Nitrobenzyl Phosphate Esters

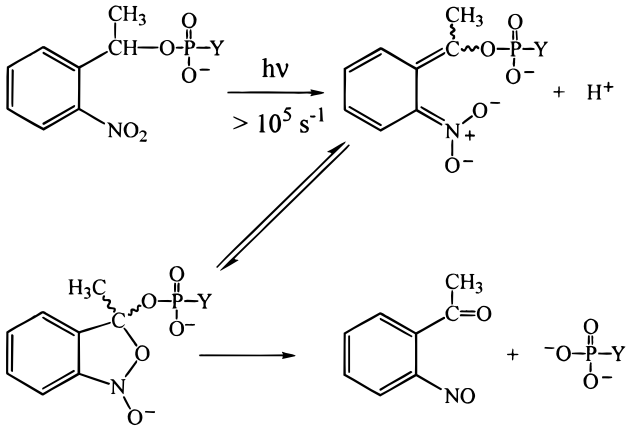

Y = OH, AMP, ADP

cases,[59,63] but it remains unclear whether several stereoisomers of the *aci*-form are involved in the reaction.

Specific acid catalysis in the *aci*-form decay was observed for several 2-nitrobenzyl phosphate esters.[60] On tenuous grounds, the catalysis has been attributed to the protonation of a phosphate group. However, acid catalysis appears to be a general phenomenon. Hess and co-workers[59] reported even more complex pH−rate profiles (curves with a minimum at pH = 7−9 or with a slope smaller than unity) for several 2-nitrobenzyl derivatives of amino acids and amides. Recently we found that a pH-profile with a minimum at pH ≈ 7.5 is also observed for 2-nitrobenzyl alcohol.[63a]

It has been reported already in 1900 that **1**, when heated in aqueous or alcoholic base, rearranges to anthranilic acid.[41a] The reaction was assumed to proceed via anthranil as an intermediate.[41] Thermal reactions affording anthranil have been reported for **1** in solution under highly acidic conditions.[42−45] Simple homolysis of the C−N bond is the favored decomposition channel of **1** in the gas phase only when the temperature is high (>1000 °C).[46,47] Anthranil formation dominates at lower temperatures. The H/D kinetic isotope effect of 1.54 observed[64] for the gas-phase decomposition of **1** indicates that H-transfer is involved in the rate-determining step. There is no direct proof that anthranil is formed through the same intermediates as the nitroso compounds in the photoreaction, but similarity of the mechanisms seems to be likely.

Thermal reactions of *o*-nitrobenzyl compounds afford a broad range of products resulting mainly from intramolecular rearrangements and condensations.[43,44] Although nitroso compounds were usually not detected in these reactions, their formation under mild conditions has been reported.[65] It is also worth mentioning that formation of anthranil derivatives in photochemical reactions of 2,2′-dinitrodiphenylmethanes has been observed.[66]

Benchmarks for the Performance of DFT Calculations. 2-Nitrotoluene has been the subject of several theoretical studies in the gas phase. Early *ab initio* studies at the SCF level were concerned mainly with the structure and energy of **1** and a few of its isomers. Surprisingly, Murray et al.[67] were not able to find any minimum for **2** at the HF/3-21G level of theory. However, they found a minimum for a conformer of **3** stabilized by 20.6 kcal mol^{-1} relative to **1**. At the HF/6-31G(d) level Chen and Wu[68] located two stationary points corresponding to a stereoisomer of **2** and a conformer of **4**. Formation of these

species from **1** involves energy changes of +43.1 and −20.0 kcal mol^{-1}, respectively. Recently, electron correlated methods were used in combination with gas-phase electron diffraction data to determine the molecular geometry of **1**.[19] None of the previous studies provided geometries and energies of 2-nitrotoluene isomers computed with electron-correlated methods or examined isomerization mechanisms by locating transition structures.

In this study we used techniques based on the density functional theory (DFT) that have been shown to yield good results for geometries, vibrational spectra, proton and electron affinities, bond energies, and other parameters of polyatomic molecules.[13b,19,23,28,31,35b,36,37b,69−78] Several theoretical studies[28,79] of CH_3NO_2 demonstrated good performance of DFT methods in predicting the geometry, vibrational frequencies, ionization, tautomerization and bond dissociation energies, and even excited-state properties of this molecule that has been considered to be "difficult" to treat with the molecular orbital theory. Numerous recent studies[19,28b,80,81] of large organic nitro compounds confirmed that DFT techniques using hybrid exchange functionals yield geometries and vibrational spectra in close agreement with experimental data and high-level ab initio calculations. DFT studies of transition structures[28,31,35b,37b,74,80,81n,82−96] did not provide such a consistent pattern of performance as those for equilibrium structures. Some results demonstrate a tendency of DFT techniques to underestimate the activation barrier heights,[82−88] especially in reactions of radical species. On the other hand, there is a growing body of evidence[28,31,35b,37b,74,80,89−96] for their accurate performance in predicting TS energies.

The hybrid DFT methods used in this work have been shown to provide reliable information on transition structures and activation barriers of pericyclic reactions and intramolecular rearrangements.[28,31,35b,74,80,92−94,96b] As an additional test we demonstrated that these techniques could predict the structure, vibrational spectrum, and dipole moment of **1** with reasonable accuracy. The B3LYP estimates obtained in this work for the equilibrium constant of the reaction **1** → *trans*-**2** and for the activation barrier of the *aci*-form cyclization are in close agreement with the QCISD(T) results. Further comparisons with available experimental and high-level ab initio data are given under Results.

Potential Energy Surface for the Reaction 1 → 4. Based on the promising results discussed above, geometry optimization at the B3LYP level using the 6-31G(d) or 6-31G(d,p) basis set was selected for a comprehensive study of the potential energy surface of **1**. This method is also expected to provide sufficient accuracy for zero-point vibrational energies. Final energies were computed with the BHLYP or B3LYP techniques using a larger basis set, such as 6-311+G(2d,p). The necessity to use two methods stems from the fact that the B3LYP method has been shown to underestimate the activation barriers for several reactions in comparison to experimental and high-level ab initio results.[83−88] In contrast, the BHLYP method appears to yield less accurate structures but energies consistent with the best estimates.[79c,80,85,88,89,96]

Both hybrid methods used yielded qualitatively consistent pictures for the landscape of the potential energy surface. However, some quantitative differences worth mentioning were found. The B3LYP method provided lower energies (here and below relative to the energy of **1**) for the quinonoid intermediates compared to the BHLYP technique. In contrast, the B3LYP energies of the conformers of **3** and **4** were found to be markedly higher in comparison to the BHLYP ones. As expected, activation barriers predicted with Becke's three-parameter functional were generally lower than those calculated with Becke's half-and-half method. However, the B3LYP activation energy for the *aci*-form cyclization was reproduced within 1.0 kcal mol^{-1} by calculating QCISD(T)/6-31G(d,p) energies at the B3LYP and MP2 geometries. The largest discrepancies between the two DFT techniques were obtained for the homolytic cleavage of the N−OH bond in **3a**. The energies of **3a** and the radical pair **5** computed with the B3LYP and BHLYP methods differ by 5.8 and 11.8 kcal mol^{-1}, respectively, the latter value being the largest discrepancy for all minimum-energy structures studied. Results of the two techniques for the energy of **TS-[3a−5]** differ even more. In fact the BHLYP method failed to give a reasonably accurate estimate for this energy as may be concluded from an unexpectedly high barrier of the reaction **5** → **3a** (radical recombination). This method also failed to provide reliable results for another diradical TS: **TS[***cis*-**2a**−*cis*-**2b]** (see Table 4).

We were able to locate several reaction paths for the conversion of **1** to **4** that is initiated by a 1,5-hydrogen shift. According to the B3LYP results, the lowest-energy path is characterized by an overall activation energy of 51.7 kcal mol^{-1}, the rate-determining step being the [1,3]H-shift in the *aci*-form **2**. The BHLYP method predicted the same rate-determining step but a higher overall barrier of 56.2 kcal mol^{-1}. The activation barrier for the reaction *cis*-**2b** → *trans*-**2** should decrease in polar solvents due to stabilization of the more polar TS. Hydrogen exchange between heteroatoms can be strongly facilitated by protic solvents. Our preliminary results[63a] obtained at the B3LYP/6-31G(d) level showed a drastic reduction of the barrier heights for the 1,3-hydrogen shift in complexes of **2b** and **3a** with a single water molecule. On the basis of these data, the rate-determining step for the formation of **4** from **2** in protic solvents is expected to be the cyclization of *trans*-**2**. However, in all cases and independent of the method used, the most favorable reaction of the *aci*-form **2** is the retautomerization to **1**. These results are consistent with experimental observations of the "photochromic", i.e., reversible, reaction of **1**.[9,51] Since the N−OH bond energy in the *aci*-form **2** is expected to be in the range 38−46 kcal mol^{-1},[28] the homolytic cleavage of this bond can hardly compete with the other reactions discussed above. We could not locate a singlet-state TS with a stable wave function that corresponds to the cis−trans isomerization of the *aci*-form by rotation around the C═N bond. This mechanism is probably of no importance for the molecules studied, since the presence of the *N*-hydroxy group is known to reduce drastically the rate of the C═N bond isomerization in the ground state.[97] Activation barriers of about 50 kcal mol^{-1} and rate constants below 10^{-13} s^{-1} were reported for oxime ethers.[97] However, this isomerization mechanism may operate in the triplet excited state. According to our results[63a] the C−N bond is strongly elongated in this state in comparison to the singlet ground state. The lowest triplet state of **1** is 53.7 kcal mol^{-1} above its ground state and 10.2 kcal mol^{-1} above the first triplet state of **2** (the most favorable cis-conformer was taken). These data were obtained at the UB3LYP/6-311+G(2d,p)//UB3LYP/6-31G(d) level of theory and corrected to the scaled zero-point vibrational energies.

The bicyclic intermediates **3** are thought to be rather labile and have never been identified in an experimental study. Related *N*-alkyl benzisoxazolines were found to be thermally labile but isolable.[98] The involvement of benzisoxazolines in the neutral or anionic form has been postulated because direct transfer of an oxygen atom or hydroxy group seems to be unlikely.

According to our DFT computations *N*-hydroxy-2,1-benzisoxazolines are, in fact, rather stable intermediates. In the gas phase, large activation barriers separate these species from **2**, **4**, and **6** (see Figure 6). This presumably holds for apolar media and indicates that isolation of such intermediates might be possible after irradiation of nitrobenzyl compounds. The B3LYP results indicate that OH radical fission from **3** may efficiently compete with the highly activated formation of **4** and the backward reaction to **2**. The N−OH bond homolysis in **3** is presumably a reaction path leading to anthranil, because the radical pair **5** should easily form an anthranil−water complex such as **9a**. According to our B3LYP calculations the effective barrier for the reaction **1** → **5** amounts to 51.7 kcal mol^{-1}. This value is in good agreement with the observed activation energies of 49.5 and 51.5 kcal mol^{-1} for anthranil formation in the gas phase.[47,64]

The *aci*-form cyclization appeared to play a key role in the mechanism and kinetics of the photoinduced isomerization of nitrobenzyl derivatives in aqueous solutions. A high activation barrier of 18.4 kcal mol^{-1} was predicted at the B3LYP/6-311+G(2d,p) level for the cyclization of *trans*-**2** in the gas phase. Based on relatively small dipole moments of both reactants and the TS, one may expect a similar barrier height for the reaction in solution.

The energy profile presented in Figure 7 shows that the reaction mechanism predicted for anionic species is essentially different from that for protonated molecules. The "cyclization" of **2**$^-$ was found to yield the anion **3**$^-$ that is structurally close to the deprotonated form of **4**. Based on the geometries of **2**$^-$ and **3**$^-$ the isomerization of the *aci*-form anion may be considered formally as an O-atom transfer. We could not locate a TS with a stable wave function for the reaction **3**$^-$ → **4**$^-$, but the barrier for this conformational change should be relatively low. Thus, the rate of the formation of the nitroso compound and of the disappearance of the *aci*-form must be the same for anions. However, the rate of product formation is expected to be much lower than that for the decay of the neutral *aci*-form.

Conclusions

The experimental gas-phase geometry and fundamental vibrational frequencies of **1** are in good agreement with those computed at the B3LYP/6-31G(d) level. Slight improvement was achieved by extending the basis set with diffuse functions on the heavy atoms and polarization functions on the hydrogens. Additional refinement of the structural parameters was obtained by using a triple-ζ like basis set. Similar effects of the basis set on the geometrical parameters were found for *trans*-**2** and **3a**. As expected, the absolute energies for all stationary points were quite sensitive to the computational method used. However, the relative energies computed with the 6-311+G(2d,p) basis set were found to be practically independent of the basis set used in the geometry optimization. Extension of the basis set to 6-311++G(3df,2p) yields no significant change in the relative energies as we showed for several selected structures.

Generally, the barriers calculated using the B3LYP functional are underestimated when compared to the BHLYP results. However, both methods provided qualitatively consistent pictures for the landscape of the potential energy surface. The theoretical results of this work are in good qualitative agreement with the available experimental results for the thermal and photoinduced isomerization of 2-nitrotoluene. An important outcome from this study is the finding that reaction pathways from **1** to **4** are essentially different for the protonated and anionic forms. Three pathways for concerted rearrangements of the neutral species were located at the B3LYP level; all of them involve the *aci*-form **2** and the bicyclic intermediate **3**. The rate-determining step is predicted to be a 1,3-hydrogen shift in **2**. A significant decrease in the activation energy of this reaction is expected in aqueous solution, so that the barrier for *aci*-form cyclization should become the highest one. In the gas phase, none of the reaction pathways leading to **4** can compete with anthranil formation initiated by N−O bond fission in **3**. For anionic species only one isomerization pathway was located. The rate-determining step was predicted to be the "cyclization" of **2**$^-$, which is the common anion for **1** and **2**. A much higher activation barrier for cyclization of the anion in comparison to that of the neutral *aci*-form suggests that specific acid catalysis should generally be observed for the decay of the anionic *aci*-form of 2-nitrobenzyl derivatives at near-neutral pH. The formation of nitroso compounds may be slower than the decay of the *aci*-form for some 2-nitrobenzyl derivatives and at low pH. In such a case specific base catalysis should be observed for product formation from the benzisoxazoline intermediates.

Supporting Information Available: Cartesian coordinates for molecules **1**−**12**, anions **2**$^-$−**4**$^-$, and 14 transition structures (ASCII); Figures 1S−12S showing the results of the IRC calculations. This material is available free of charge via the Internet at http://pubs.acs.org.

References and Notes

(1) (a) Barltrop, J. A.; Plant, P. J.; Schofield, P. *J. Chem. Soc., Chem. Commun.* **1966**, 822−823. (b) Patchornik, A.; Amit, B.; Woodward, R. B. *J. Am. Chem. Soc.* **1970**, *92*, 6333−6335. (c) Zehavi, U.; Amit, B.; Patchornik, A. *J. Org. Chem.* **1972**, *37*, 2281−2285. (d) Hébert, J.; Gravel, D. *Can. J. Chem.* **1974**, *52*, 187−189. (e) Gravel, D.; Murray, S.; Ladouceur, G. *J. Chem. Soc., Chem. Commun.* **1985**, 1828−1829. (f) Rich, D. H., Gurwara, S. K. *J. Am. Chem. Soc.* **1975**, *97*, 1575−1579. (g) Rodebaugh, R.; Fraser-Reid, B.; Geysen, H. M. *Tetrahedron Lett.* **1997**, *38*, 7653−7656. (h) Whitehouse, D. L., Savinov, S. N.; Austin, D. J. *Tetrahedron Lett.* **1997**, *38*, 7851−7652.

(2) Beecher, J. E.; Cameron, J. F.; Fréchet, J. M. J. *J. Mater. Chem.* **1992**, *2*, 811−816.

(3) (a) Kubota, S.; Tanaka, Y.; Moriwaki, T.; Eto, S. *J. Electrochem. Soc.* **1991**, *138*, 1080−1084. (b) Houlihan, F. M.; Nalamasu, O.; Kometani, J. M.; Reichmanis, E. *J. Imaging Sci. Technol.* **1997**, *41*, 35−40 and references therein.

(4) For reviews, see: Marriot, G., Ed. *Methods Enzymol.* **1998**, *291*, 1−259 and references therein.

(5) (a) Lester, H. A.; Nerbonne, J. M. *Annu. Rev. Biophys. Bioeng.* **1982**, *11*, 151−175. (b) Gurney, A. M.; Lester, H. A. *Physiol. Rev.* **1987**, *67*, 583−617.

(6) McCray, J. A.; Trentham, D. R. *Annu. Rev. Biophys. Biophys. Chem.* **1989**, *18*, 239−270.

(7) Adams, S. R.; Tsien, R. Y. *Annu. Rev. Physiol.* **1993**, *55*, 755−784.

(8) (a) McCray, J. A.; Fidler-Lim, N.; Ellis-Davies, G. C. R.; Kaplan, J. H. *Biochemistry* **1992**, *31*, 8856−8861. (b) Khan, S.; Castellano, F.; Spudich, J. L.; McCray, J. A.; Goody, R. S.; Reid, G. P.; Trentham, D. R. *Biophys. J.* **1993**, *65*, 2368−2382. (c) Walker, J. W.; Martin, H.; Schmitt, F. R.; Barsotti, R. J. *Biochemistry* **1993**, *32*, 1338−1345. (d) Marriott, G.; Heidecker, M. *Biochemistry* **1996**, *35*, 3170−3174. (e) Niu, L.; Gee, K. R.; Schaper, K.; Hess, G. P. *Biochemistry* **1996**, *35*, 2030−2036. (f) Pan, P.; Bayley, H. *FEBS Lett.* **1997**, *405*, 81−85. (g) Cohen, B. E.; Stoddard, B. L.; Koshland, D. E., Jr. *Biochemistry* **1997**, *36*, 9035−9044. (h) Rossi, F. M.; Margulis, M.; Tang, C.-M.; Kao, J. P. Y. *J. Biol. Chem.* **1997**, *272*, 32933−32939. (i) Chaulk, S. G.; MacMillan, A. M. *Nucleic Acids Res.* **1998**, *26*, 3173−3178. (j) Papageorgiou, G.; Ogden, D. C.; Barth, A.; Corrie, J. E. T. *J. Am. Chem. Soc.* **1999**, *121*, 6503−6504.

(9) (a) Wettermark, G. *J. Phys. Chem.* **1962**, *66*, 2560−2562. (b) Wettermark, G.; Black, E.; Dogliotti, L. *Photochem. Photobiol.* **1965**, *4*, 229−239.

(10) Frisch, M. J.; Trucks, G. W.; Schlegel, H. B.; Gill, P. M. W.; Johnson, B. G.; Robb, M. A.; Cheeseman, J. R.; Keith, T.; Petersson, G. A.; Montgomery, J. A.; Raghavachari, K.; Al-Laham, M. A.; Zakrzewski, V. G.; Ortiz, J. V.; Foresman, J. B.; Cioslowski, J.; Stefanov, B. B.; Nanayakkara, A.; Challacombe, M.; Peng, C. Y.; Ayala, P. Y.; Chen, W.; Wong, M. W.; Andres, J. L.; Replogle, E. S.; Gomperts, R.; Martin, R. L.; Fox, D. J.; Binkley, J. S.; Defrees, D. J.; Baker, J.; Stewart, J. P.; Head-Gordon, M.; Gonzalez, C.; Pople, J. A. *GAUSSIAN 94*, Revision B.2, Gaussian, Inc.: Pittsburgh, PA, 1995.

(11) Frisch, M. J.; Trucks, G. W.; Schlegel, H. B.; Scuseria, G. E.; Robb, M. A.: Cheeseman, J. R.; Zakrzewski, V. G.; Montgomery, J. A.; Stratmann, R. E., Jr.; Burant, J. C.; Dapprich, S.; Millam, J. M.; Daniels, A. D.; Kudin, K. N.; Strain, M. C.; Farkas, O.; Tomasi, J.; Barone, V.; Cossi, M.; Cammi, R.; Mennucci, B.; Pomelli, C.; Adamo, C.; Clifford, S.; Ochterski, J.; Petersson, G. A.; Ayala, P. Y.; Cui, Q.; Morokuma, K.; Malick, D. K.; Rabuck, A. D.; Raghavachari, K.; Foresman, J. B.; Cioslowski, J.; Ortiz, J. V.; Stefanov, B. B.; Liu, G.; Liashenko, A.; Piskorz, P.; Komaromi, I.; Gomperts, R.; Martin, R. L.; Fox, D. J.; Keith, T.; Al-Laham, M. A.; Peng, C. Y.; Nanayakkara, A.; Gonzalez, C.; Challacombe, M.; Gill, P. M. W.; Johnson, B.; Chen, W.; Wong, M. W.; Andres, J. L.; Gonzalez, C.; Head-Gordon, M.; Replogle, E. S.; Pople, J. A. *GAUSSIAN 98*, Revision A.5, Gaussian, Inc.: Pittsburgh, PA, 1998.

(12) Becke, A. D. *J. Chem. Phys.* **1993**, *98*, 5648−5652.

(13) (a) Lee, C.; Yang, W.; Parr, R. G. *Phys. Rev. B* **1988**, *37*, 785−797. (b) Stephens, P. J.; Devlin, F. J.; Chabalowski, C. F.; Frisch M. J. *J. Phys. Chem.* **1994**, *98*, 11623−11627.

(14) (a) Perdew, J. P.; Wang, Y. *Phys. Rev.* **1992**, *B45*, 13244−13255. (b) Perdew, J. P.; Chavary, J. A.; Vosko, S. H.; Jackson, K. A.; Pederson, M. R.; Singh, D. J.; Fiolhais, C. *Phys. Rev.* **1992**, *B46*, 6671−6679.

(15) Becke, A. D. *J. Chem. Phys.* **1993**, *98*, 1372−1377.

(16) Pople, J. A.; Head-Gordon, M.; Raghavachari, K. *J. Chem. Phys.* **1987**, *87*, 5968−5975.

(17) Peng, C.; Schlegel, H. B. *Isr. J. Chem.* **1993**, *33*, 449−454.

(18) (a) Fukui, K. *Acc. Chem. Res.* **1981**, *14*, 363−368. (b) Gonzalez, C.; Schlegel, H. B. *J. Phys. Chem.* **1990**, *94*, 5523−5527.

(19) Shishkov, I. F.; Vilkov, L. V.; Kovács, A.; Hargittai, I. *J. Mol. Struct.* **1998**, *445*, 259−268.

(20) Hargittai, M.; Hargittai, I. *Int. J. Quantum Chem.* **1992**, *44*, 1057−1067.

(21) (a) Carper, W. R.; Davis, L. P.; Extine, M. W. *J. Phys. Chem.* **1981**, *86*, 459−462. (b) Nash, C. P.; Nelson, T. E.; Stewart, J. J. P.; Carper, W. R. *Spectrochim. Acta* **1989**, *45A*, 585−588.

(22) Green, J. H. S.; Harrison, D. J. *Spectrochim. Acta* **1970**, *26A*, 1925−1937.

(23) (a) Pople, J. A.; Scott, A. P.; Wong, M. W.; Radom, L. *Isr. J. Chem.* **1993**, *33*, 345−350. (b) Scott, A. P.; Radom, L. *J. Phys. Chem.* **1996**, *100*, 16502−16513. (c) Wong, M. W. *Chem. Phys. Lett.* **1996**, *256*, 391−399.

(24) Heilbronner, E.; Schmelzer, A. *Nouv. J. Chim.* **1980**, 23−28.

(25) (a) Franc, J. *Coll. Czech. Chem. Commun.* **1961**, *26*, 596−598. (b) Cheng, L.-T.; Tam, W.; Stevenson, S. H.; Meredith, G. R.; Rikken, G.; Marder, S. R. *J. Phys. Chem.* **1991**, *95*, 10631−10643.

(26) (a) Powell, D. R.; Hanson, P. E.; Gellman, S. H. *Acta Crystallogr.* **1996**, *C52*, 2945−2946. (b) Colvin, E. W.; Beck, A. K.; Bastani, B.; Seebach, D.; Kai, Y.; Dunitz, J. D. *Helv. Chim. Acta* **1980**, *63*, 697−710.

(27) Lelievre, J.; Farrell, P. G.; Terrier, F. *J. Chem. Soc., Perkin Trans. 2* **1986**, 333−336.

(28) (a) Lammertsma, K.; Prasad, B. V. *J. Am. Chem. Soc.* **1993**, *115*, 2348−2351. (b) Harris, N. J.; Lammertsma, K. *J. Am. Chem. Soc.* **1996**, *118*, 8048−8055.

(29) McKee, M. L. *J. Am. Chem. Soc.* **1986**, *108*, 5784−5792.

(30) Mebel, A. M.; Hsu, C.-C.; Lin, M. C.; Morokuma, K. *J. Chem. Phys.* **1995**, *103*, 5640−5649.

(31) Jursic, B. S. *Chem. Phys. Lett.* **1999**, *299*, 334−344.

(32) Tsunekawa *J. Phys. Soc. Jpn.* **1972**, *33*, 167−175.

(33) (a) Grünanger, P., Vita-Finzi, P., Eds. In: *Isoxazoles Part I*; Wiley & Sons: New York, 1991; pp 677−725 and references therein. (b) Grünanger, P., Vita-Finzi, P., Eds. In: *Isoxazoles Part II*; John Wiley & Sons: New York, 1999; pp 822−827.

(34) Kostyanovsky, R. G.; Rudchenko, V. F.; D'yachenko, O. A.; Chervin, I. I.; Zolotoi, A. B.; Atovmyan, L. O. *Tetrahedron* **1979**, *35*, 213−224.

(35) (a) Chung-Phillips, A.; Jebber, K. A. *J. Chem. Phys.* **1995**, *102*, 7080−7087. (b) Boulet, P.; Gilardoni, F.; Weber, J.; Chermette, H.; Ellinger, Y. *Chem. Phys.* **1999**, *244*, 163−174.

(36) Hsu, C.-C.; Lin, M. C.; Mebel, A. M.; Melius, C. F. *J. Phys. Chem. A* **1997**, *101*, 60−66.

(37) (a) Adeney, P. D.; Bouma, W. J.; Radom, L.; Rodwell, W. R. *J. Am. Chem. Soc.* **1980**, *102*, 4069−4074. (b) Vladimiroff, T. *J. Mol. Struct.* **1997**, *401*, 141−150.

(38) (a) Hanyu, Y.; Boggs, J. E. *J. Chem. Phys.* **1965**, *43*, 3454−3456. (b) Hanyu, Y.; Britt, C. O.; Boggs, J. E. *J. Chem. Phys.* **1966**, *45*, 4725−4747.

(39) Sakaizumi, T.; Usami, A.; Satoh, H.; Ohashi, O.; Yamaguchi, I. *J. Mol. Spectrosc.* **1994**, *164*, 536−549.

(40) Turner, P. H.; Cox, A. P. *J. Chem. Soc., Faraday Trans. 2* **1978**, *74*, 533−559.

(41) (a) Preuss, L.; Binz, A. *Z. Angew. Chem.* **1900**, *13*, 385−386. (b) Bakke, J.; Heikman, H.; Nystrøm, G. *Acta Chem. Scand.* **1972**, *26*, 355−364. (c) Willadsen, P.; Zerner, B.; MacDonald, C. G. *J. Org. Chem.* **1973**, *38*, 3411−3412.

(42) Eckroth, D. R.; Cochran, T. G. *J. Chem. Soc. C.*, **1970**, 2660−2661.

(43) (a) Wünsch, K.-H.; Boulton, A. J. *Adv. Heterocycl. Chem.* **1967**, *8*, 277−379. (b) Smalley, R. K. *Adv. Heterocycl. Chem.* **1981**, *29*, 1−69.

(44) Preston, P. N.; Tennant, G. *Chem. Rev.* **1972**, *72*, 627−677 and references therein.

(45) (a) Austin, R. P.; Ridd, J. H. *J. Chem. Soc., Chem. Commun.* **1992**, 1599. (b) Austin, R. P.; Ridd, J. H. *J. Chem. Soc., Perkin Trans. 2* **1994**, 1205−1210. (c) Austin, R. P.; Ridd, J. H. *J. Chem. Soc., Perkin Trans. 2* **1994**, 1411−1414.

(46) Brill, T. B.; James, K. J. *Chem. Rev.* **1993**, *93*, 2667−2692 and references therein.

(47) (a) Tsang, W.; Robaugh, D.; Mallard, W. G. *J. Phys. Chem.* **1986**, *90*, 5968−5973. (b) He, Y. Z.; Cui, J. P.; Mallard, W. G.; Tsang, W. *J. Am. Chem. Soc.* **1988**, *110*, 3754−3759.

(48) Morrison, H.; Migdalof, B. H. *J. Org. Chem.* **1965**, *30*, 3996−3997.

(49) Morrison, H. A. In: *The Chemistry of Functional Groups, The Chemistry of the Nitro and Nitroso Groups*; Feuer, H., Ed.; Wiley & Sons: New York, 1969; Chapter 4.

(50) (a) Yip, R. W.; Sharma, D. K.; Giasson, R.; Gravel, D. *J. Phys. Chem.* **1984**, *88*, 5770−5772. (b) Gravel, D.; Giasson, R.; Blanchet, D.; Yip, R. W.; Sharma, D. K. *Can. J. Chem.* **1991**, *69*, 1193−1200.

(51) Nurmukhametov, R. N.; Sergeev, A. M. *Russ. J. Phys. Chem. (Engl. Transl.)* **1990**, *64*, 163−171.

(52) (a) Wettermark, G.; Ricci, R. *J. Chem. Phys.* **1963**, *39*, 1218−1223. (b) Langmuir, M. E.; Dogliotti, L.; Black, E. D.; Wettermark, G. *J. Am. Chem. Soc.* **1969**, *91*, 2204−2207.

(53) (a) Atherton, S. J.; Craig, B. B. *Chem. Phys. Lett.* **1986**, *127*, 7−12. (b) Chattopadhyay, S. K.; Craig, B. B. *J. Phys. Chem.* **1987**, *91*, 323−326.

(54) McClelland, R. A.; Steenken, S. *Can. J. Chem.* **1987**, *65*, 353−356.

(55) (a) Suryanarayanan, K.; Capellos, C. *Int. J. Chem. Kinetics* **1974**, *6*, 89−102. (b) Burlinson, N. E.; Sitzman, M. E.; Kaplan, L .A.; Kayser, E. *J. Org. Chem.* **1979**, *44*, 3695−3698.

(56) (a) Yip, R. W.; Sharma, D. K.; Giasson, R.; Gravel, D. *J. Phys. Chem.* **1985**, *89*, 5328−5330. (b) Yip, R. W.; Wen, Y. X.; Gravel, D.; Giasson, R.; Sharma, D. K. *J. Phys. Chem.* **1991**, *95*, 6078−6081.

(57) (a) Margerum, J. D.; Miller, L. J.; Saito, E.; Brown, M. S.; Mosher, H. S.; Hardwick, R. *J. Phys. Chem.* **1962**, *66*, 2434−2438. (b) Bluhm, A. L.; Sousa, J. A.; Weinstein, J. *J. Org. Chem.* **1964**, *29*, 636−640. (c) Sixl, H.; Warta, R. *Chem. Phys.* **1985**, *94*, 147−155. (d) Corval, A.; Kuldova, K.; Eichen, Y.; Pikramenou, Z.; Lehn, J. M.; Trommsdorff, H. P. *J. Phys. Chem.* **1996**, *100*, 19315−19320.

(58) (a) Schupp, H.; Wong, W. K.; Schnabel, W. *J. Photochem.* **1987**, *36*, 85−97. (b) Zhu, Q. Q.; Schnabel, W.; Schupp, H. *J. Photochem.* **1987**, *39*, 317−332.

(59) (a) Walker, J. W.; McCray, J. A.; Hess, G. P. *Biochemistry* **1986**, *25*, 1799−1805. (b) Milburn, T.; Matsubara, N.; Billington, A. P.; Udgaonkar, J. B.; Walker, J. W.; Carpenter, B. K.; Webb, W. W.; Marque, J.; Denk, W.; McCray, J. A.; Hess, G. P. *Biochemistry* **1989**, *28*, 49−55. (c) Billington, A. P.; Walstrom, K. M.; Ramesh, D.; Guzikowski, A. P.; Carpenter, B. K.; Hess, G. P. *Biochemistry* **1992**, *31*, 5500−5507. (d) Ramesh, D.; Wieboldt, R.; Billington, A. P.; Carpenter, B. K.; Hess, G. P. *J. Org. Chem.* **1993**, *58*, 4599−4605. (e) Gee, K. R.; Wieboldt, R.; Hess, G. P. *J. Am. Chem. Soc.* **1994**, *116*, 8366−8367.

(60) (a) McCray, J. A.; Trentham, D. R. *Biophys. J.* **1985**, *47*, 406a. (b) Walker, J. W.; Reid, G. P.; McCray, J. A.; Trentham, D. R. *J. Am. Chem. Soc.* **1988**, *110*, 7170−7177.

(61) (a) Barth, A.; Hauser, K.; Mäntele, W.; Corrie, J. E. T.; Trentham, D. R. *J. Am. Chem. Soc.* **1995**, *117*, 10311−10316. (b) Barth, A.; Corrie, J. E. T.; Gradwell, M .J.; Maeda, Y.; Mäntele, W.; Meier, T.; Trentham, D. R. *J. Am. Chem. Soc.* **1997**, *119*, 4149−4159. (c) Rammelsberg, R.; Boulas, S.; Chorongiewski, H.; Gerwert, K. *Vibr. Spectrosc.* **1999**, *19*, 143−149.

(62) Nielsen, A. T. In: *Nitrones, Nitronates and Nitroxides*; Patai, S., Ed.; Wiley & Sons: Chichester, 1989; pp 2−138.

(63) (a) Il'ichev, Yu. V.; Wirz, J. Unpublished results. (b) Schaper, K., Düsseldorf, personal communication.

(64) Matveev, V. G.; Dubikhin, V. V.; Nazin, G. M. *Izv. Akad. Nauk SSSR, Ser. Khim. (in Russian)* **1978**, 474−477.

(65) (a) Ohwada, T.; Kasuga, M.; Shudo, K. *J. Org. Chem.* **1990**, *55*, 2717−2719. (b) Chen, L.-J.; Burka, L .T. *Tetrahedron Lett.* **1998**, *39*, 5351−5354. (c) Corrie, J. E. T.; Gradwell, M. J.; Papageorgiou, G. *J. Chem. Soc., Perkin Trans. 1* **1999**, 2977−2982.

(66) (a) Joshua, C. P.; Ramdas, P. K. *Tetrahedron Lett.* **1974**, *49*, 4359−4360. (b) Christudhas, M.; Joshua, C. P. *Aust. J. Chem.* **1982**, *35*, 2377−2381.

(67) Murray, J. S.; Lane, P.; Politzer, P.; Bolduc, P. R.; McKenney, R. L., Jr. *J. Mol. Struct.* **1990**, *209*, 349−359.

(68) Chen, P. C.; Wu, C. W. *J. Mol. Struct.* **1995**, *357*, 87−95.

(69) (a) Gill, P. M. W.; Johnson, B. G.; Pople, J. A.; Frish, M. J. *Chem. Phys. Lett.* **1992**, *197*, 499−505. (b) Johnson, B. G.; Gill, P. M. W.; Pople, J. A. *J. Chem. Phys.* **1993**, *98*, 5612−5626. (c) Curtiss, L. A.; Raghavachari, K.; Redfern, P. C.; Pople, J. A. *J. Chem. Phys.* **1997**, *106*, 1063−1079.

(70) (a) Pulay, P.; Fogarasi, G.; Pongor, G.; Boggs, J. E.; Vargha, A. *J. Am. Chem. Soc.* **1983**, *105*, 7037−7047. (b) Rauhut, G.; Pulay, P. *J. Phys. Chem.* **1995**, *99*, 3093−3100. (c) Rauhut, G.; Jarzecki, A. A.; Pulay, P. *J. Comput Chem.* **1997**, *18*, 489−500.

(71) Petersson, G. A.; Malick, D. K.; Wilson, W. G.; Ochterski, J. W.; Montgomery, J. A.; Frisch M. J. *J. Chem. Phys.* **1998**, *109*, 10570−10579.

(72) Kohn, W.; Becke, A. D.; Parr, R. G. *J. Phys. Chem.* **1996**, *100*, 12974−12980 and references therein.

(73) Friesner, R. A.; Murphy R. B.; Beachy M. D.; Ringnalda M. N.; Pollard W. T.; Dunietz B. D.; Cao Y. *J. Phys. Chem. A* **1999**, *103* , 1913−1928.

(74) (a) Jursic, B. S. *Chem. Phys. Lett.* **1995**, *236*, 206−210. (b) Jursic, B. S. *Chem. Phys. Lett.* **1996**, *256*, 213−219. (c) Jursic, B. S. *Chem. Phys. Lett.* **1996**, *256*, 603−608. (d) Jursic, B. S. *Chem. Phys. Lett.* **1996**, *261*, 13−17. (e) Jursic, B. S. *J. Mol. Struct.* **1998**, *428*, 41−47.

(75) (a) El-Azhary, A. A.; Suter, H. U. *J. Phys. Chem.* **1996**, *100*, 15056−15063. (b) Devlin F. J.; Stephens P. J.; Cheeseman J. R.; Frisch M. J. *J. Phys. Chem. A* **1997**, *101*, 6322−6333. (c) Langhoff, S. R.; Bauschlicher, C. W., Jr.; Hudgins, D. M.; Sandford, S. A.; Allamandola, L. J. *J. Phys. Chem. A* **1998**, *102*, 1632−1646.

(76) (a) Halls, M. D.; Schlegel, H. B. *J. Chem. Phys.* **1998**, *109*, 10587−10593. (b) Halls, M. D.; Schlegel, H. B. *J. Chem. Phys.* **1999**, *111*, 8819−8824.

(77) (a) Smith, B. J.; Radom, L. *Chem. Phys. Lett.* **1995**, *245*, 123−128. (b) DiLabio, G. A.; Pratt, D. A.; LoFaro, A. D.; Wright, J .S. *J. Phys. Chem. A* **1999**, *103*, 1653−1661.

(78) (a) de Oliveira, G.; Martin, J. M. L.; de Proft, F.; Geerlings, P. *Phys. Rev.* **1999**, *60*, 1034−1045. (b) VanLier, G.; DeProft, F.; Geerlings, P *Chem. Phys. Lett.* **1997,** *274*, 396−404.

(79) (a) Redington, P. K.; Andzelm, J. W. In: *Density Functional Methods in Chemistry*; Labanowski, J. K., Andzelm, J. W., Eds.; Springer: New York, 1991; pp 411−418. (b) Gutsev, G. L.; Bartlett, R. J. *J. Chem. Phys.* **1996,** *105*, 8785−8792. (c) Jursic, B. S. *Int. J. Quantum Chem.* **1997,** *64*, 263−269. (d) Manaa, M. R.; Fried, L. E. *J. Phys. Chem. A* **1998,** *102*, 9884−9889. (e) Thümmel, H. T. *J. Phys. Chem. A* **1998**, *102*, 2002-2008. (f) Wiener, J. J. M.; Politzer, P. *J. Mol. Struct.* **1998**, *427*, 171-174.

(80) (a) Rauhut, G. *J. Comput. Chem.* **1996**, *17*, 1848−1856. (b) Eckert, F.; Rauhut, G. *J. Am. Chem. Soc.* **1998**, *120*, 13478−13484. (c) Eckert, F.; Rauhut, G.; Katritzky, A. R.; Steel, P. J. *J. Am. Chem. Soc.* **1999**, *121*, 6700−6711. (d) Rauhut, G.; Eckert, F. *J. Phys. Chem.* **1999**, *103*, 9086−9092.

(81) (a) Sorescu, D. C.; Sutton, T. R. L.; Thompson, D. L.; Beardall, D.; Wight, C. A. *J. Mol. Struct.* **1996**, *384*, 87−99. (b) Sorescu, D. C.; Bennett, C. M.; Thompson, D. L. *J. Phys. Chem. A* **1998**, *102*, 10348−10357. (c) Rice, B. M.; Chabalowski C. F. *J. Phys. Chem. A* **1997**, *101*, 8720−8726. (d) Wu, C. J.; Fried, L. E. *J. Phys. Chem. A* **1997,** *101*, 8675−8679. (e) Harris, N. J.; Lammertsma, K. *J. Am. Chem. Soc.* **1997**, *119*, 6583−6589. (f) Vladimiroff, T. *J. Mol. Struct.* **1998,** *453*, 119−122. (g) Cho, S. G.; Cheun, Y. G.; Park, B. S. *J. Mol. Struct.* **1998,** *432*, 41−53. (h) Cho, S. G.; Park, B. S. *Int. J. Quantum Chem.* **1999**, *72*, 145−154. (i) Politzer, P.; Concha, M. C.; Grice, M. E.; Murray, J. S.; Lane, P.; Habibollazadeh, D. *J. Mol. Strucutre* **1998**, *452*, 75−83. (j) Kovacs, A.; Izvekov, V.; Keresztury, G.; Pongor, G. *Chem. Phys.* **1998**, *238*, 231−243. (k) Chen, P. C.; Tzeng, S. C. *J. Mol. Struct.* **1999,** *467*, 243−257. (l) Urbanowicz, P.; Kupka, T.; Wrzalik, R.; Pasterny, K. *J. Mol. Struct.* **1999**, *483*, 409−414. (m) Juranyi, F.; Keresztury, G. *J. Mol. Struct.* **1999**, *483*, 443−447. (n) Johnson, M. A.; Truong, T. N. *J. Phys. Chem. A* **1999**, *103*, 8840−8846.

(82) Johnson, B. G.; Gonzales, C. A.; Gill, P. M. W.; Pople, J. A. *Chem. Phys. Lett.* **1992**, *221*, 100−108.

(83) Glukhovtsev, M. N.; Bach, R. D.; Pross, A.; Radom, L. *Chem. Phys. Lett.* **1996**, *260*, 558−564.

(84) Basch H.; Hoz S. *J. Phys. Chem. A* **1997**, *101*, 4416−4431.

(85) Durant, J. L. *Chem. Phys. Lett.* **1996**, *256*, 595−602.

(86) (a) Baker, J.; Muir, M.; Andzelm, J. *J. Chem. Phys.* **1995**, *102*, 2063−2079. (b) Baker, J.; Andzelm, J.; Muir, M.; Taylor, P. R. *Chem. Phys. Lett.* **1995**, *237*, 53−60.

(87) (a) Zhang, Q.; Bell, R.; Truong, T. N. *J. Phys. Chem.* **1995**, *99*, 592−599. (b) Bell, R. L.; Taveras, D. L.; Truong, T. N.; Simons. J. *Int. J. Quantum Chem.* **1997**, *63*, 861−874.

(88) Zhang, Y.; Zhao, C. Y.; Fang, W. H.; Lu, Z. H. *J. Mol. Struct.* **1998**, *454*, 31−40.

(89) (a) Pai, S. V.; Chabalowski C. F.; Rice B. M. *J. Phys. Chem.* **1996**, *100*, 15368−15382. (b) Rice B. M.; Pai S. V.; Chabalowski C. F. *J. Phys. Chem. A* **1998**, *102*, 6950−6956.

(90) (a) Bernardi, F.; Bottoni, A. *J. Phys. Chem. A* **1997**, *101*, 1912−1919. (b) Bottoni, A. *J. Phys. Chem. A* **1998**, *102*, 10142−10150.

(91) (a) Wong, M. W.; Radom, L. *J. Phys. Chem. A* **1998**, *102*, 2237−2245. (b) Barone, V.; Orlandini, L. *Chem. Phys. Lett.* **1995**, *246*, 45−52.

(92) (a) Wiest, O.; Houk, K. N. *Topics Curr. Chem.* **1996**, *183*, 2−22 and references therein. (b) Wiest, O.; Montiel, D. C.; Houk, K. N. *J. Phys. Chem. A* **1997**, *101*, 8378−8388.

(93) (a) Gridnev, I. D.; Tok, O. L.; Gridneva, N. A.; Bubnov, Y. N.; Schreiner, P. R. *J. Am. Chem. Soc.* **1998**, *120*, 1034−1043. (b) Gridnev, I. D.; Schreiner, P. R.; Gurskii, M. E.; Bubnov, Y. N.; Krasavin, A. O.; Mstislavski, V. I. *Chem. Commun.* **1998**, 2507−2508.

(94) Fernández−Ramos, A.; Smedarchina, Z., Siebrand, W.; Zgierski, M. Z.; Rios, M. A. *J. Am. Chem. Soc.* **1999**, *121*, 6280−6289.

(95) (a) Sosa, C.; Andzelm, J.; Lee, C.; Blake, J. F.; Chenard, B. L.; Butler, T. W. *Int. J. Quantum Chem.* **1994**, *49*, 511−526. (b) Magnuson, E. C.; Pranata, J. *J. Comput. Chem.* **1998**, *19*, 1795−1804. (c) Freccero, M.; Gandolfi, R.; Sarzi−Amadè, M.; Rastelli, A. *J. Chem. Soc., Perkin Trans. 2* **1998**, 2413−2419.

(96) (a) Bach, R. D.; Glukhovtsev, M. N.; Gonzalez, C.; Marquez, M.; Estevez, C. M.; Baboul, A. G.; Schlegel, H. B. *J. Phys. Chem. A* **1997**, *101*, 6092−6100. (b) Baboul, A. G.; Schlegel, H. B.; Glukhovtsev, M. N.; Bach, R. D. *J. Comput. Chem.* **1998**, *19*, 1353−1369.

(97) (a) Padwa, A. *Chem. Rev.* **1977**, *77*, 37−68. (b) Arai, T.; Furuya, Y.; Furuuchi, H.; Tokumaru, K. *Chem. Phys. Lett.* **1993**, *212*, 597−603. (c) Arai, T.; Tokumaru, K. *Adv. Photochem.* **1995**, *20*, 1−57.

(98) (a) Olofson, R. A.; Vander Meer, R. K.; Stournas, S. *J. Am. Chem. Soc.* **1971**, *93*, 1543−1544. (b) Nakagawa, Y.; Aki, O.; Sirakawa, K. *Chem. Pharm. Bull.* **1972**, *20*, 2209−2214. (c) Coombs, R. V. *J. Org. Chem.* **1977**, *42*, 1812−1813. (d) Haley, N. F. *J. Org. Chem.* **1978**, *43*, 1233−1237.